# Supplementary Information

## Influence of the pendant groups on electrochemical water oxidation catalyzed by cobalt(II) triazolylpyridine complexes

Bo-Hong Luo, Si-Yang Zhao, Yong-Li Pu, Xiang-Yu Zhou, Jun-Zhou Xie, Long Chen, Min Wu, Min Zhou and Hua-Xin Zhang*

*College of Chemistry and Chemical Engineering, Guangxi University, No. 100, Daxue East Road, Nanning 530004, Guangxi, China*

* Corresponding author.
*E-mail address*: zhanghx@gxu.edu.cn (H.-X. Zhang).

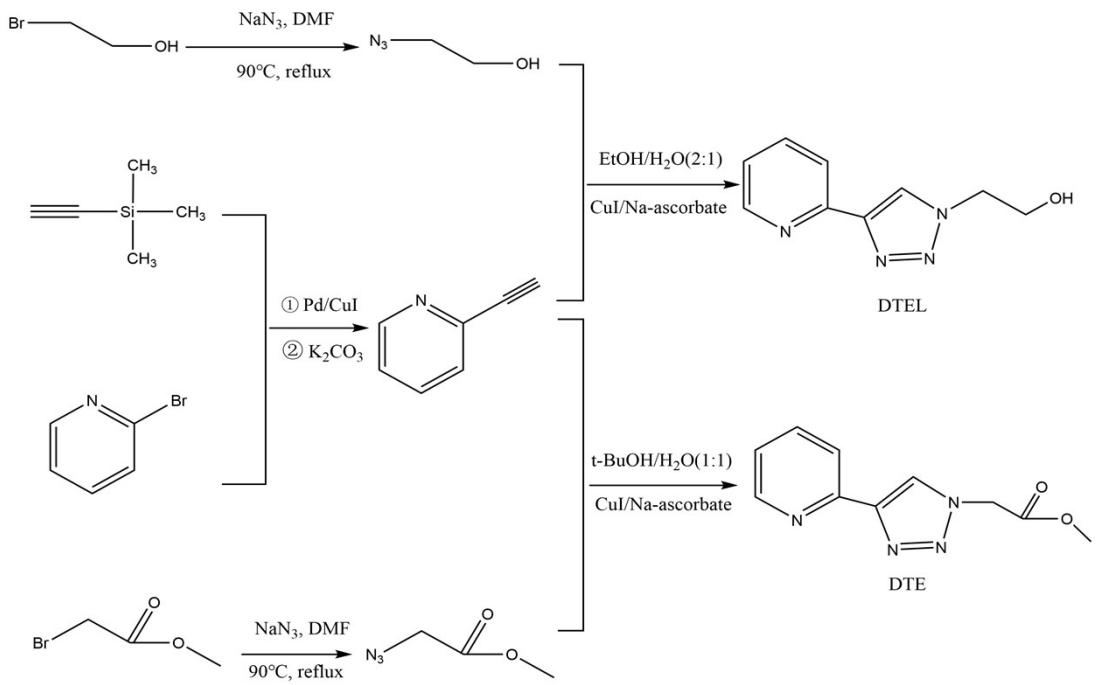


Scheme 1: Synthetic routes of DTE and DTEL

**Synthesis**

**1-(2-acetoxymethyl)-4-(2-pyridyl)1,2,3-triazole (DTE).**

2-Methyl azidoacetate (1000 mg, 9.7 mmol) and 2-ethynylpyridine (1170 mg, 10.18 mmol) were dissolved in a mixture of water/*tert*-butanol (70 mL, 1:1, v/v). The solution was purged with $N_2$ for 30 min. Then cuprous iodide (277.0 mg, 1.46 mmol) and sodium ascorbate (288.0 mg, 1.46 mmol) was added. The reaction solution was bubbled with $N_2$ for another 10 minutes and then stirred under $N_2$ atmosphere at room temperature for 24 hrs. The resulting solution was diluted with 50 mL water and extracted with dichloromethane. The organic layer was washed with water and brine, dried over anhydrous sodium sulfate, and filtered. The solvent of the filtrate was evaporated to give a yellow-brown solid, which was purified by silica gel column chromatography with an eluent (n-hexane:ethyl acetate, 4:1, v/v). A light yellow solid was obtained. Yield: 1320 mg, 63%. $^1$HNMR (400 MHz, in $CDCl_3$,): δ 3.84 (3H，O-$CH_3$), 5.26 (2H, $CH_2$), 7.81 (dt, 1H), 8.20 (dt, 1H), 8.29 (1H), 8.62 (ddd, 1H). IR (KBr pellet, $cm^{-1}$): 3496w, 3000w, 2938w, 1750s, 1600s, 1230s, 785s, 997s.

**1-(2-hydroxy)-4-(2-pyridyl)1,2,3-triazole (DTEL).**

2-Ethynylpyridine (1000 mg, 9.7 mmol) and azidoethanol (1370 mg, 15.68 mmol) were dissolved in a mixture of water/ethanol (60 mL, 2:1, v/v). The solution was purged with $N_2$ for 30 min. Then cuprous iodide (426.0 mg, 2.23 mmol) and sodium ascorbate (443.0 mg, 2.23 mmol) was added. The reaction solution was bubbled with $N_2$ for another 10 minutes and then stirred under $N_2$ atmosphere at room temperature for 24 hrs. The reaction solution was filtered and the solvent of the filtrate was removed to obtain a brown-yellow solid, which was purified by silica gel column chromatography with an eluent (dichloromethane: methanol, 50:1, v/v). A white solid was obtained. Yield: 1290 mg, 70%. $^1$HNMR (400 MHz, in $CDCl_3$) δ 8.50 (dd, 1H), 8.32 (s, 1H), 8.09 (dd, 1H), 7.78 (dt, 1H), 7.29 (ddd, 1H), 4.57 (dd, 2H), 4.17 (dd, 2H). IR (KBr pellet, $cm^{-1}$): 3226w, 3123w, 1607s, 1419s, 1077s, 785s, 997s.

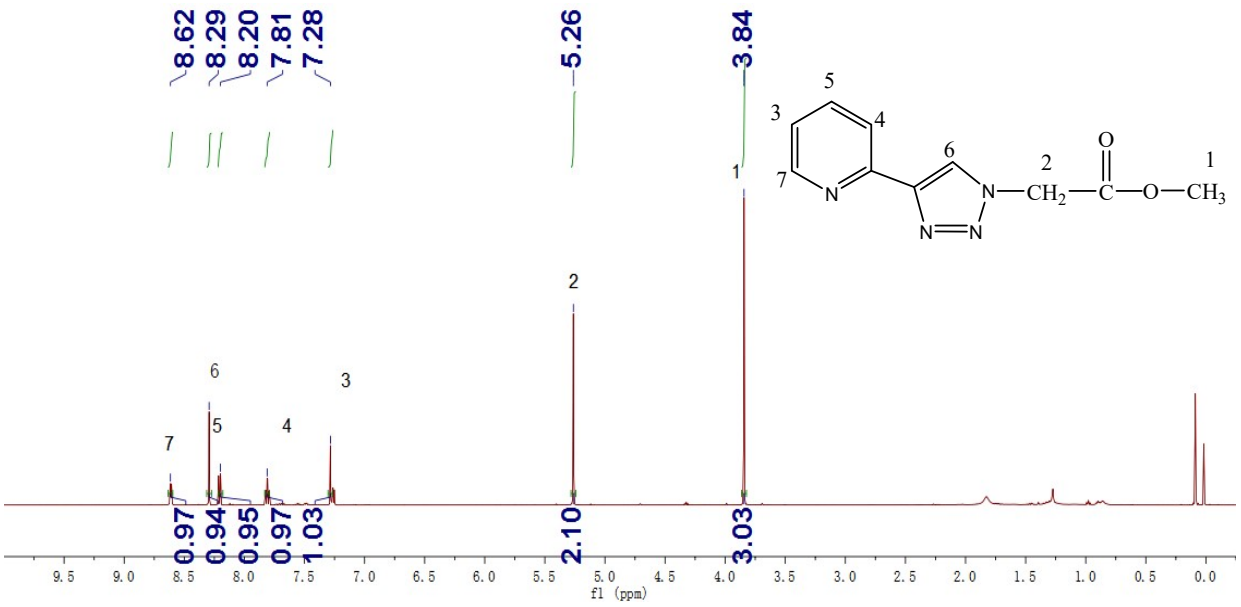


Fig. S1 $^{1}$H NMR spectrum of DTE in $CDCl_3$.

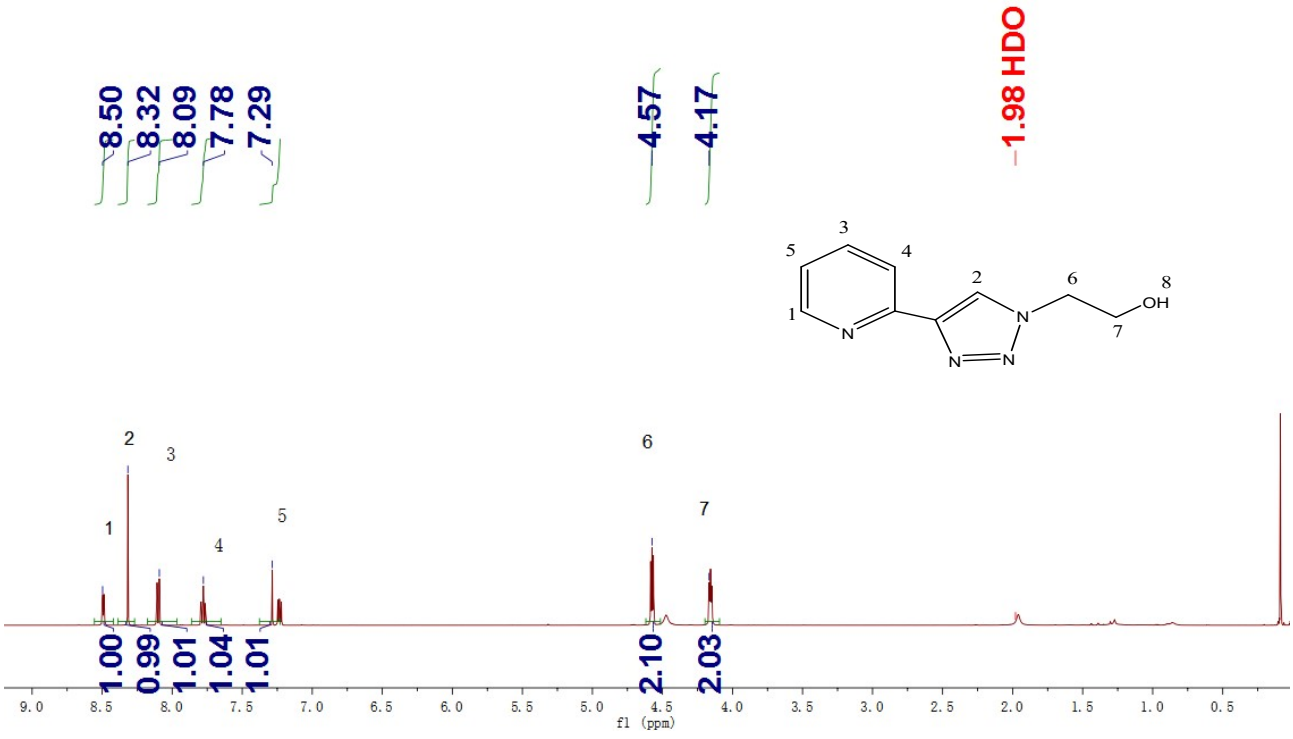


Fig. S2 $^{1}$HNMR spectrum of DTEL in $CDCl_3$

Table S1 Crystallographic data and structure refinement parameters for **1-3**

| Complex | **1** | **2** | **3** |
|---|---|---|---|
| Empirical formula | $CoC_{23}H_{28}N_8Cl_2O_{15}$ | $CoC_{22}H_{28}Cl_2N_8O_6$ | $CoC_{20}H_{28}N_8\ Cl_2O_{12}$ |
| Formula weight | 786.36 | 630.36 | 702.33 |
| Temperature / K | 293(2) | 293(2) | 293(2) |
| Crystal system | orthorhombic | triclinic | triclinic |
| Space group | $Pca2_1$ | P-1 | P-1 |
| *a* /Å | 16.6231(3) | 8.2052(5) | 8.2037(3) |
| *b* /Å | 8.2700(2) | 8.6632(5) | 8.8646(4) |
| *c* /Å | 24.4235(4) | 11.9123(4) | 10.5178(5) |
| *Z* | 4 | 2 | 2 |
| *α* / ° | 90 | 86.849(4) | 80.730(4) |
| *β* / ° | 90 | 75.453(4) | 87.961(3) |
| *γ* / ° | 90 | 62.022(6) | 77.741(4) |
| Crystal size/mm | 0.15 × 0.08 × 0.06 | 0.21× 0.19 × 0.15 | 0.25 × 0.23 × 0.17 |
| Absorption coefficient/$mm^{-1}$ | 0.750 | 6.774 | 0.835 |
| *h* | $-19 \le h \le 19$ | $-10 \le h \le 10$ | $-10 \le h \le 11$ |
| *k* | $-9 \le k \le 9$ | $-8 \le h \le 10$ | $-11 \le h \le 11$ |
| *l* | $-29 \le l \le 29$ | $-14 \le h \le 14$ | $-13 \le h \le 14$ |
| *F*(000) | 1612 | 305 | 361 |
| *θ* for data collection/° | 1.668–25.342 | 3.844-75.512 | 3.459-28.858 |
| Reflections collected/unique | 36027[*R*(int)= 0.0567] | 6604[*R*(int)= 0.0471] | 11402[*R*(int)= 0.0268] |
| Data/ restraints / parameters | 6110/1/443 | 2766/0/178 | 3507/0/197 |
| Goodness-of-fit on $F^2$ | 1.072 | 1.052 | 1.070 |
| Final *R* indices [$I > 2\sigma(I)$] | $R_1 = 0.0747$ $wR_2 = 0.1801$ | $R_1 = 0.0592$ $wR_2 = 0.1662$ | $R_1 = 0.0435$ $wR_2 = 0.1187$ |
| Residual electron density/eV | 0.51 | 0.84 | 0.79 |

Table S2 Selected bond lengths (Å) and bond angles (º) for **1**

| | | | |
|---|---|---|---|
| Co1-N1 | 2.121(5) | Co1-N2 | 2.078(6) |
| Co1-N5 | 2.164(5) | Co1-N6 | 2.123(5) |
| Co1-O1 | 2.143(5) | Co1-O2 | 2.088(5) |
| N2 -Co1-N1 | 77.58(19) | N5-Co1-N1 | 175.50(19) |
| N6 -Co1-N1 | 104.06(18) | N6-Co1-N2 | 177.8(2) |
| N6 -Co1-N5 | 76.58(19) | N2-Co1-N5 | 101.7(2) |
| O1-Co1-N2 | 88.6(2) | O1-Co1-N5 | 88.17(18) |
| O1-Co1-O2 | 178.6(2) | N2-Co1-O2 | 92.0(2) |
| N5-Co1-O2 | 92.93(19) | N6-Co1-O2 | 89.4(2) |
| O2-Co1-N1 | 91.53(19) | N6-Co1-O1 | 90.0(2) |
| O1-Co1-N1 | 87.37(18) | | |

Table S3 Selected bond lengths (Å) and bond angles (º) for **2**

| | | | |
|---|---|---|---|
| Co1-N1 | 2.132(2) | Co1-N2 | 2.137(2) |
| Co1-N1[1] | 2.132(2) | Co1-N2[1] | 2.137(2) |
| Co1-Cl1 | 2.4598(8) | Co1-Cl1[1] | 2.4598(8) |
| N2-Co1-N2[1] | 180.0 | N1-Co1-N2 | 77.03(9) |
| N2[1]-Co1-N1 | 102.97(9) | N1[1]-Co1-N2 | 102.97(11) |
| N2[1]-Co1-N1[1] | 77.03(9) | N1-Co1-N1[1] | 180.0 |
| N2-Co1-Cl1 | 89.12(7) | N2[1]-Co1-Cl1 | 90.88(7) |
| N1-Co1-Cl1 | 89.53(7) | N1[1]-Co1-Cl1 | 90.47(7) |
| N2-Co1-Cl1[1] | 90.88(7) | N2[1]-Co1-Cl1[1] | 89.12(7) |
| N1-Co1-Cl1[1] | 90.47(7) | N1[1]-Co1-Cl1[1] | 89.53(9) |
| Cl1-Co1-Cl1[1] | 180.0 | | |

Symmetry code: 1-*x,* 1-*y,* 1-*x*

Table S4 Selected bond lengths (Å) and bond angles (º) for **3**

| | | | |
|---|---|---|---|
| Co1-O2 | 2.0946(18) | Co1-O2[1] | 2.0946(18) |
| Co1-N2 | 2.120(2) | Co1-N2[1] | 2.120(2) |
| Co1-N5 | 2.135(2) | Co1-N5[1] | 2.135(2） |
| O2A-Co1-O2 | 180.0 | O2-Co1-N5[1] | 90.65(8) |
| O2[1]-Co1-N5 | 90.65(8) | O2[1]-Co1-N5[1] | 89.35(8) |
| O2-Co1-N5 | 89.35(8) | N5-Co1-N5[1] | 180.0 |
| O2[1]-Co1-N2[1] | 88.61(8) | O2-Co1-N2[1] | 91.39(8) |
| O2-Co1-N2 | 88.61(8) | O2[1]-Co1-N2 | 91.39(8) |
| N2-Co1-N5 | 77.33(8) | N2-Co1-N5[1] | 102.67(8) |
| N2[1]-Co1-N5 | 102.67(8) | N2[1]-Co1-N5[1] | 77.33(8) |
| N2-Co1-N2[1] | 180.0 | | |

Symmetry code: 1-*x,* 1-*y,* 1-*x*

Table S5 Comparison of overpotential ($\eta$), rate constant ($k_{cat}$) and Faradaic efficiency (FE) for WOR catalyzed by **1**-**4** and other catalysts based on mononuclear cobalt complexes.

| Catalyst | pH | Conditions | $\eta$/mV | $k_{cat}/s^{-1}$ | FE/% | Ref. |
|---|---|---|---|---|---|---|
| **1** | 7.0 | 0.1 M acetate buffer | 480 | 0.53 | 92 | This work |
| **2** | 7.0 | 0.1 M acetate buffer | 440 | 0.96 | 86 | This work |
| **3** | 7.0 | 0.1 M acetate buffer | 440 | 0.21 | 80 | This work |
| **4** | 7.0 | 0.1 M acetate buffer | 480 | 0.48 | 77 | This work |
| $Co(bipyalk)(OAc)_2$ | 7.0 | 0.1 M borate buffer | 330 | – | 94 | S1 |
| Co–L1 | 7.0 | 0.1 M borate buffer | 450 | – | ~90 | S2 |
| Co–L2 | 7.0 | 0.1 M borate buffer | ~580 | – | ~90 | S3 |
| $[Co(N_3Py_2)(H_2O)](ClO_4)_2$ | 9.0 | 0.1 M borate buffer | 540 | 0.79 | 97 | S4 |
| $CoH^{\beta F}CX\text{-}CO_2H$ | 7.0 | 0.1 M phosphate buffer | 780 | 0.81 | – | S5 |
| $[Co^{III}(dpaq)(Cl)]Cl$ | 8.0 | 0.1 M phosphate buffer | 500 | 85 | 81 | S6 |
| $Co^{II}(TCA)_2(H_2O)_2$ | 6.0 | 0.1 M acetate buffer | 360 | – | – | S7 |
| $[Co(Py_5)(OH_2)]^{2+}$ | 9.2 | 0.1 M phosphate buffer | 500 | 79 | – | S8 |
| $[Co(bpbH_2)Cl_2]$ | 8.6 | 0.25 M phosphate buffer | 560 | 81.54 | 98.5 | S9 |
| $Na[L_3Co^{III}]$ | 7.0 | 0.1 M phosphate buffer | 380 | 7.53 | ~90 | S10 |
| $[Co(tpfc)(py)_2]$ | 7.0 | 0.1 M borate buffer | – | 0.20 | ~95 | S11 |
| $(Et_4N)[Co^{III}\text{-bTAML}]$ | 9.2 | 0.1 M phosphate buffer | – | 5.68 | 62 | S12 |
| $[Co(tip(Me))(MeCN)]^{2+}$ | 9.2 | 0.1 M phosphate buffer | 500 | | 99.8 | S13 |

The onset potential for WOR ($E_{onset}$) in this work was defined as the point at which $i_c/i_{pa} = 2$ during the cyclic voltammetry measurements using glassy carbon at 100 $mV.s^{-1}$, where $i_c$ was the current observed in the presence of the complex under $N_2$, $i_{pa}$ was the oxidative peak current of the redox wave of $Cu^{II}/Cu^{I}$ (Figure 3a). The overpotential ($\eta$) was calculated according to the equation: $\eta$ (V) = $E_{onset}$ (V vs. Ag/AgCl) + 0.197 V + 0.059 V × pH – 1.23 V.

bipyalk = 2,2'-([2,2'-bipyridine]-6,6'-diyl)bis(propan-2-ol), OAc = acetate

L1 = 5,15-bis-(pentafluorophenyl)-10-(4-dibenzofuran)corrole

L2 = 5,10,15,20-tetrakis-(1,3-dimethylimidazolium-2-yl)porphyrin

$N_3Py_2$ = 2,5,8-trimethyl-1,9-bis(2-pyridyl)-2,5,8-triazanonane

$H^{\beta F}CX\text{-}CO_2H$ = 2,3,7,8,12,13,17,18-octafluoro-10-(4-(5-hydroxycarbonyl-2,7-di-tert-9,9-dimethyl-xanthene))-5,15-bis(pentafluorophenyl)corrole

H-dpaq = 2-[bis(pyridin-2-ylmethyl)]amino-N-quinolin-8-yl-acetamidate

TCA = 1-mesityl-1,2,3-1*H*-triazole-4-carboxylate

Py5 = 2,6-(bis(bis-2-pyridyl)-methoxy-methane)pyridine

$bpbH_2$ = N,N'-bis(2'-pyridinecarboxamide)-1,2-benzene

L3 = *o*-benzoquinonedicarboxamido

tpfc = 5,10,15-tris(pentafluorophenyl)corrole, py = pyridine

bTAML = biuret-modified tetraamidomacrocyclic

tip(Me) = 2,6-(bis(bis-2-N-methyl-imidazole)-hydroxymethyl)pyridine

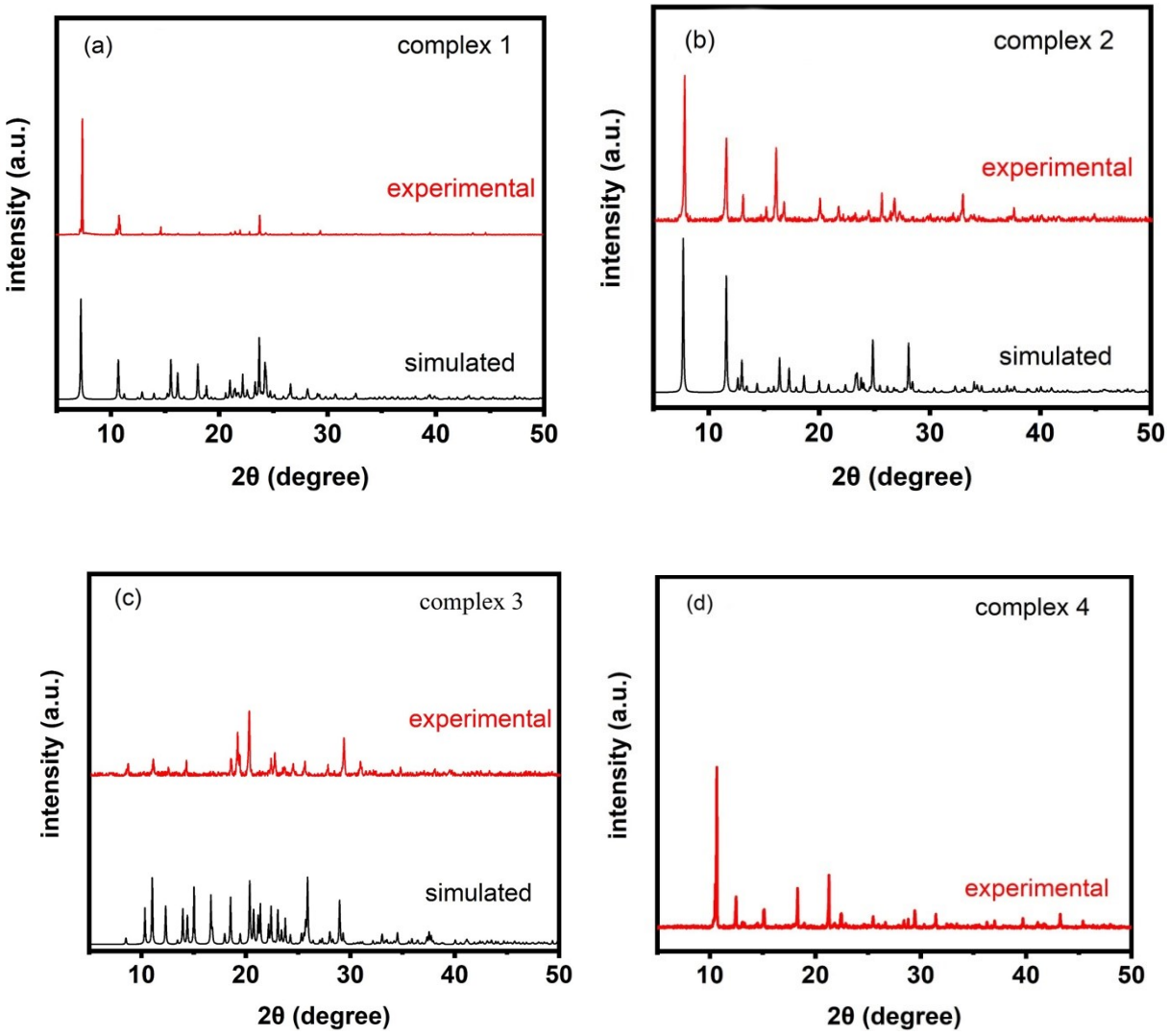


Fig. S3 Powder X-ray diffraction (PXRD) patterns of complexes (a) **1**, (b) **2**, (c) **3** and (d) **4**: simulated data (black) and measured data (red).

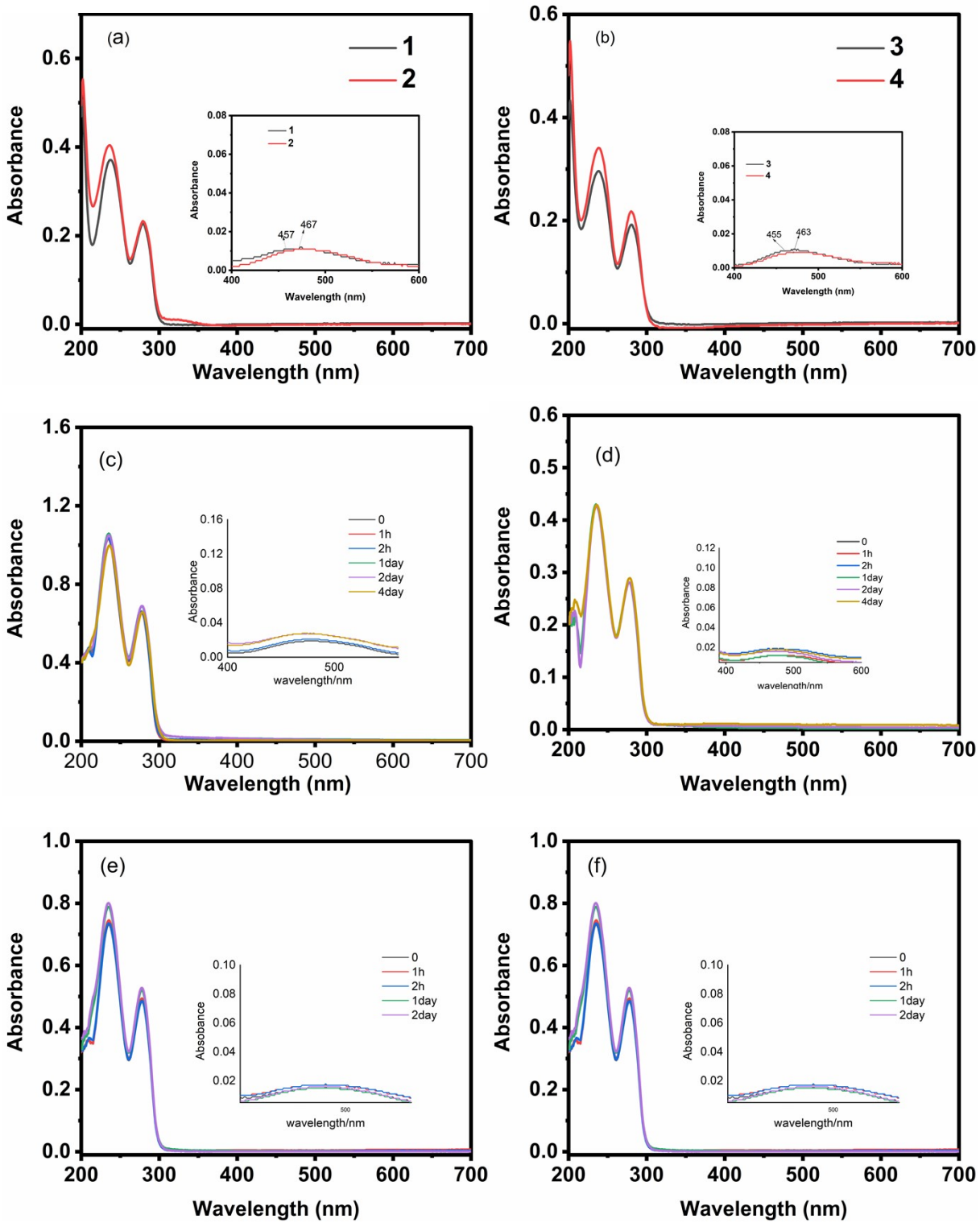


Fig. S4 UV−vis spectra of (a) **1**, **2** and (b) **3**, **4** in methanol solutions. Time-dependent UV−vis spectra of (c) **1**, (d) **2**, (e) **3**, (f) **4** in pH 7.0 0.1 M NaOAc-HOAc solutions. Inset: Magnified view of the band in the region 400–600 nm, sample concentration: 1.0 mM.

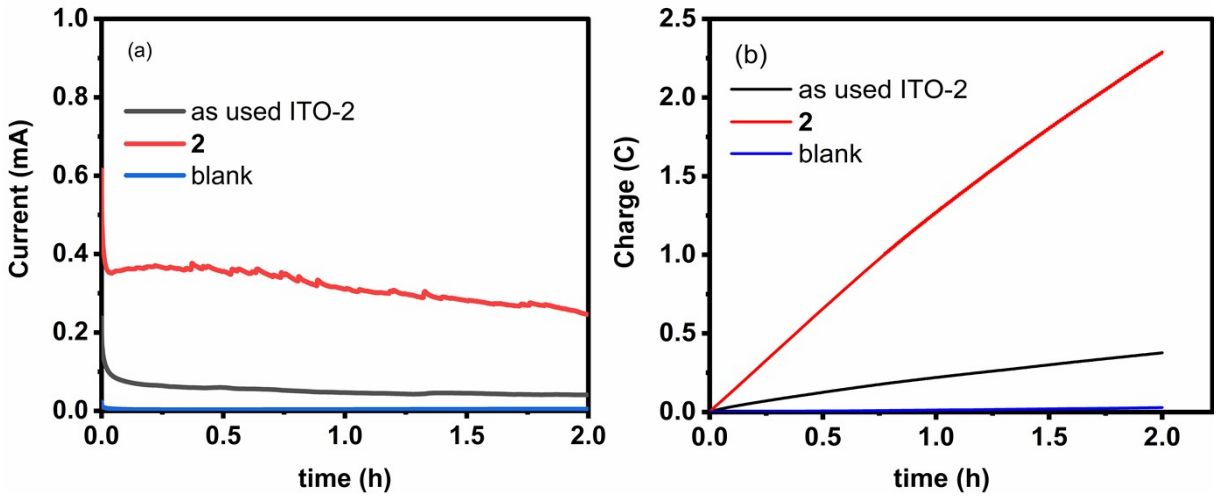


Fig. S5 (a) I–t curves and (b) charge buildup during controlled potential electrolysis in pH 7.0 0.1 M NaOAc-HOAc solution using ITO as the working electrode at 1.40 V. Red line for the solution with **2** (0.4 mM), black line for the used ITO electrode in blank solution, blue line for the blank solution.

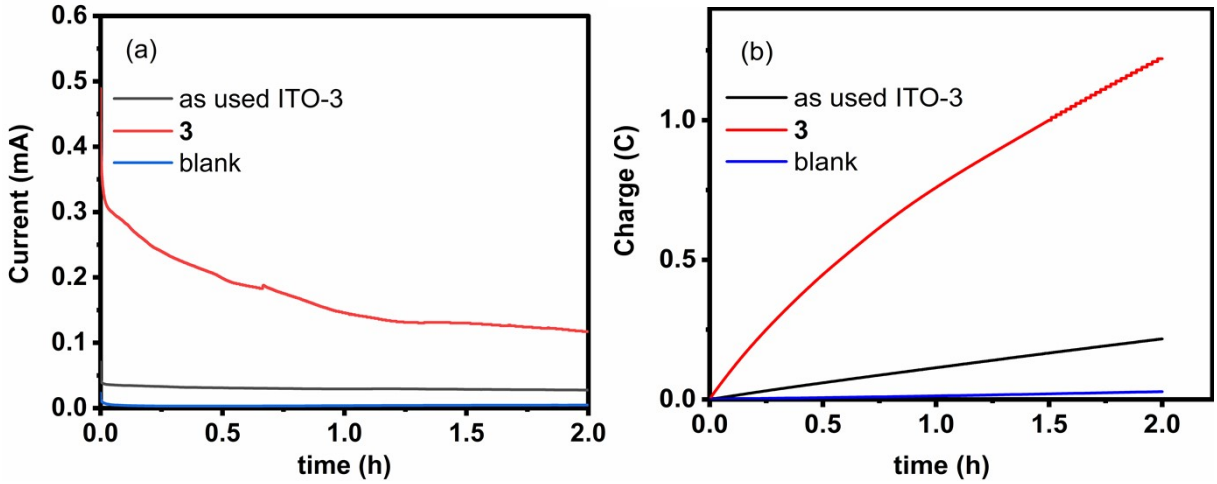


Fig. S6 (a) I–t curves and (b) charge buildup during controlled potential electrolysis in 0.1 M NaOAc-HOAc solution at pH 7.0 using ITO as the working electrode at 1.40 V. Red line for the solution with **3** (0.4 mM), black line for the used ITO electrode in blank solution, blue line for the blank solution.

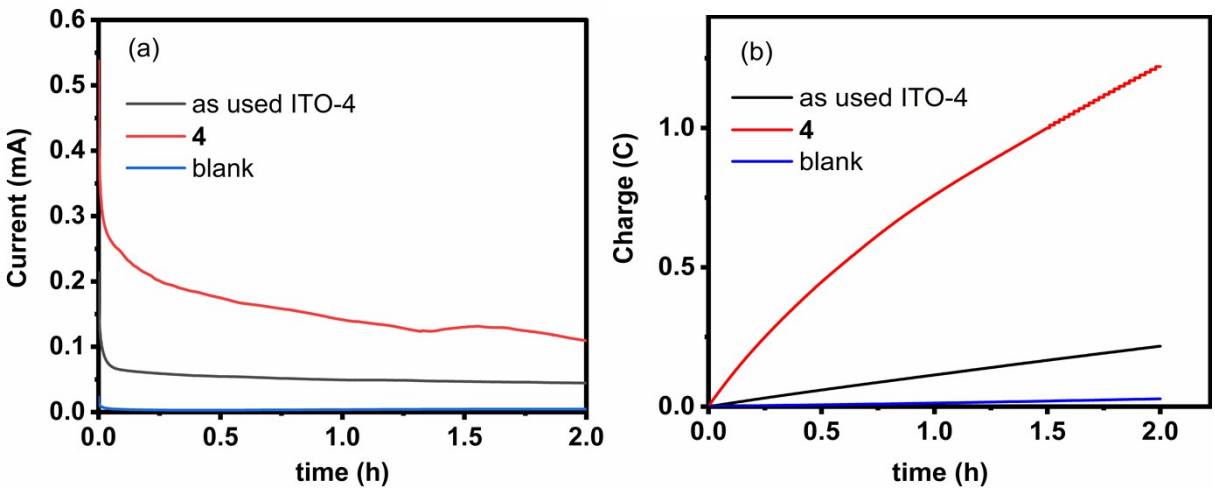


Fig. S7 (a) I–t curves and (b) charge buildup during controlled potential electrolysis in 0.1 M NaOAc-HOAc solution at pH 7.0 using ITO as the working electrode at 1.40 V. Red line for the solution with **4** (0.4 mM), black line for the used ITO electrode in blank solution, blue line for the blank solution.

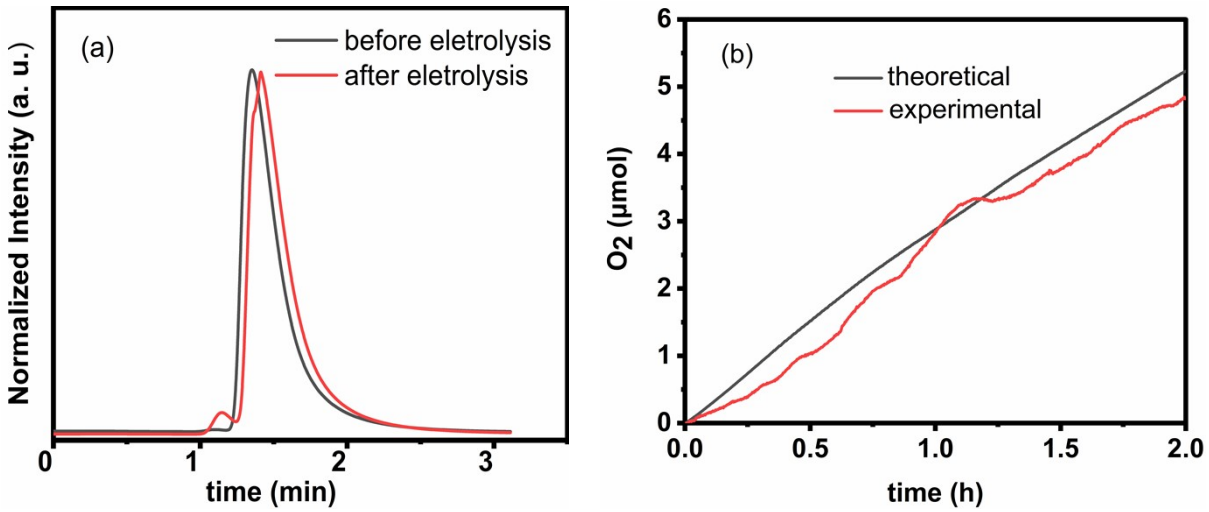


Fig. S8 (a) Traces from gas chromatography before (black line) and after (red line) the electrolysis of **1** (0.4 mM) in pH 7.0 0.1 M NaOAc-HAc solution using ITO as working electrode at 1.40 V. (b) Oxygen-evolving trace obtained from the electrolysis of **1** under the same condition of (a).

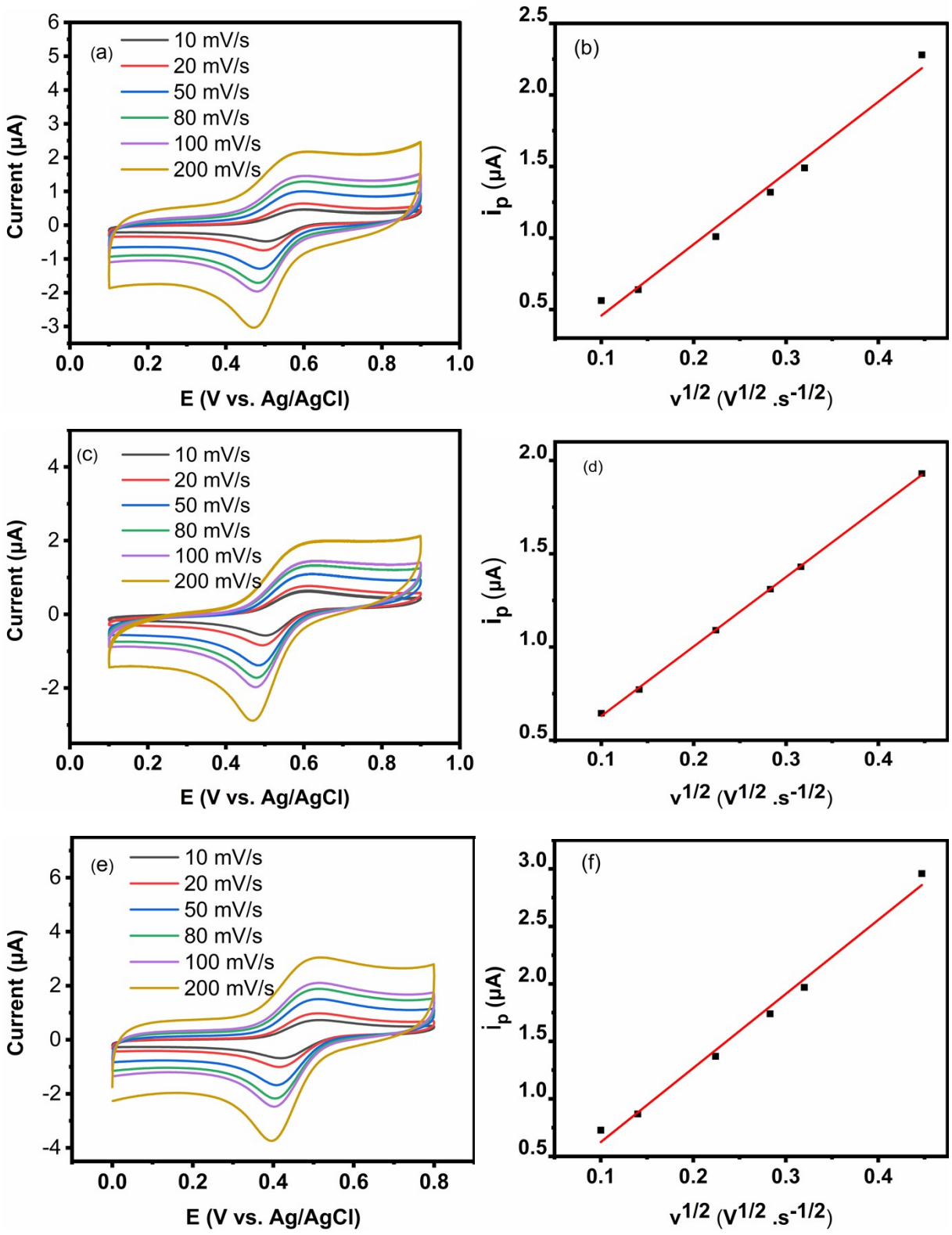
(a)
10 mV/s
20 mV/s
50 mV/s
80 mV/s
100 mV/s
200 mV/s
Current (μA)
E (V vs. Ag/AgCl)
(b)
$i_p$ (μA)
$v^{1/2}$ ($V^{1/2}$ .$s^{-1/2}$)
(c)
10 mV/s
20 mV/s
50 mV/s
80 mV/s
100 mV/s
200 mV/s
Current (μA)
E (V vs. Ag/AgCl)
(d)
$i_p$ (μA)
$v^{1/2}$ ($V^{1/2}$ .$s^{-1/2}$)
(e)
10 mV/s
20 mV/s
50 mV/s
80 mV/s
100 mV/s
200 mV/s
Current (μA)
E (V vs. Ag/AgCl)
(f)
$i_p$ (μA)
$v^{1/2}$ ($V^{1/2}$ .$s^{-1/2}$)

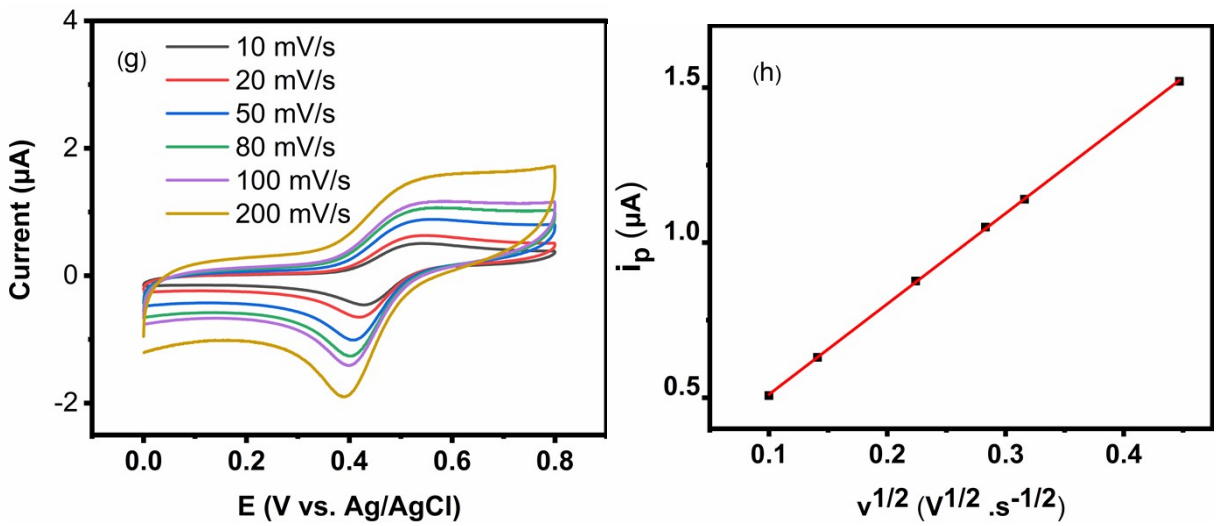


Fig. S9 CVs of (a) **1**, (c) **2**，(e) **3** and (g) **4** in pH 7.0 0.1 M NaOAc–HOAc solutions at variable scan rates. Working electrode: glassy carbon. Concentration of sample: 0.40 mM. Plot of $i_p$ vs $v^{1/2}$ for (b) **1**, (d) **2**, (f) **3** and (h) **4**, where $i_p$ was measured at 0.60 V.

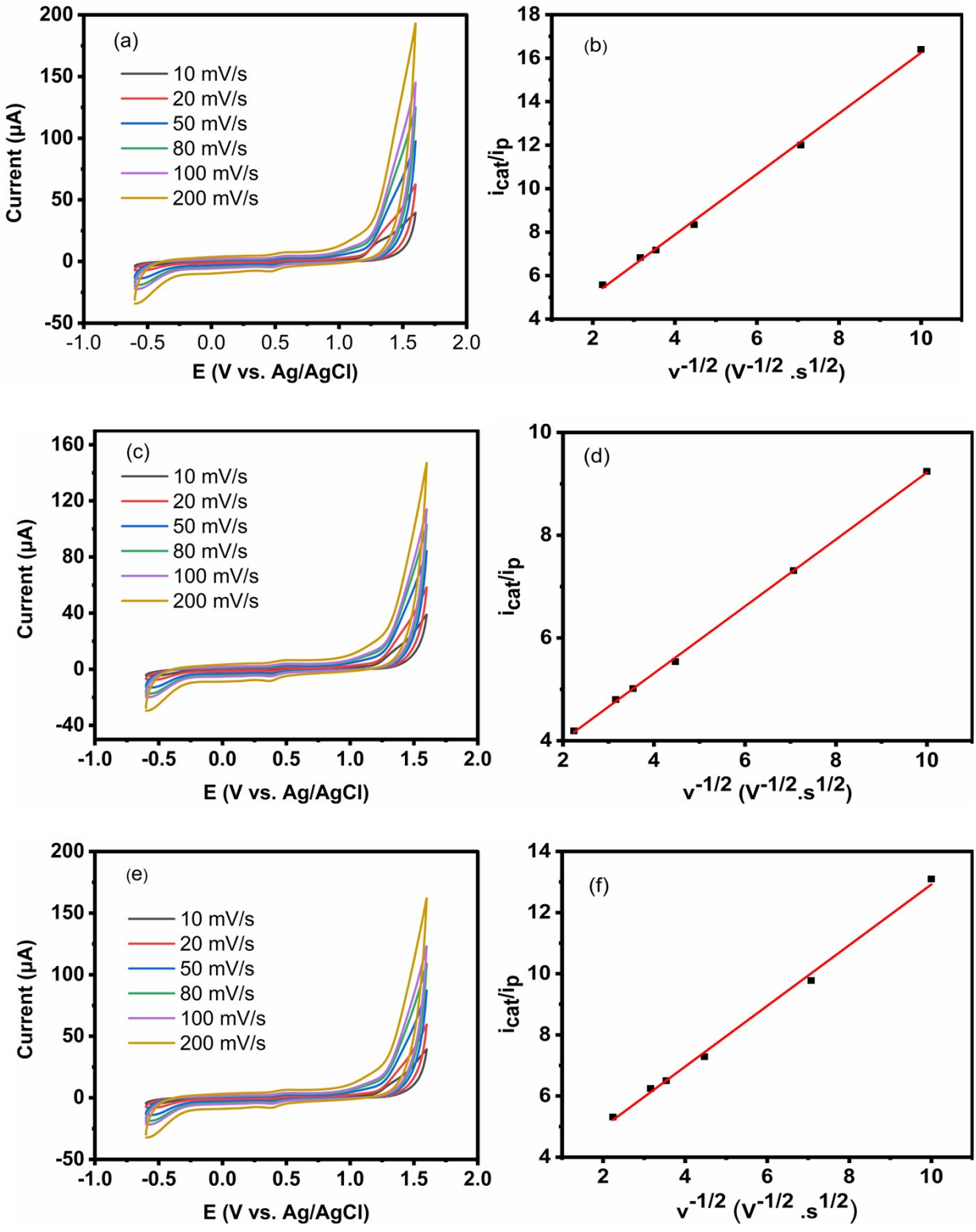


Fig. S10 CVs of (a) **2**, (c) **3** and (e) **4** in pH 7.0 0.1 M NaOAc–HOAc solutions at different scan rates. Concentration of sample: 0.40 mM. Working electrode: glassy carbon. Plot of the ratio of $i_{cat}/i_p$ as a function of $v^{-1/2}$ for (b) **2**, (d) **3** and (f) **4**, where $i_{cat}$ was measured at 1.28 V and $i_p$ was measured at 0.60 V.

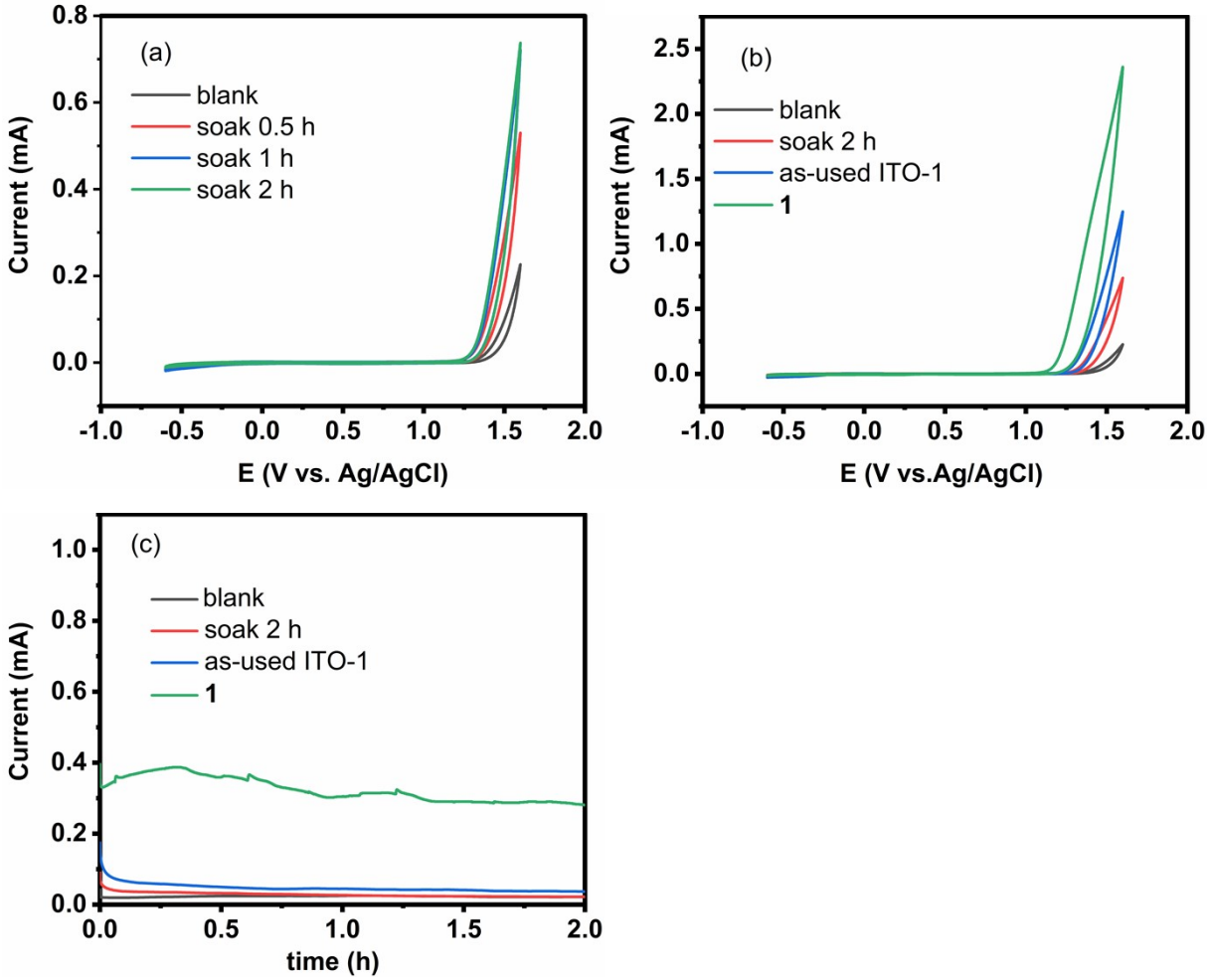


Fig. S11 (a) CVs in pH 7.0 0.1 M NaOAc-HOAc blank solution using ITO electrode soaked in the solution of **1** (0.4 mM) for different time as working electrodes. Scan rate: 100 mV $s^{-1}$. (b) CVs in pH 7.0 0.1 M NaOAc-HOAc blank solution using ITO electrode soaked in the solution of **1** (0.4 mM) for 2 hours as working electrode, using the rinsed ITO electrode after the electrolysis of **1** at 1.40 V for 2 hours (as used ITO-1) as working electrode, using a fresh ITO as working electrode. CV of the solution of complex **1** using a fresh ITO as working electrode was shown for comparison. Scan rate: 100 mV $s^{-1}$. (c) I-t curves obtained from CPE at 1.4 V in pH 7.0 0.1 M NaOAc-HOAc blank solution using ITO electrode soaked in the solution of **1** (0.4 mM) for 2 hours as working electrode, using the rinsed ITO electrode after the electrolysis of **1** at 1.40 V for 2 hours (as used ITO-1) as working electrode, using a fresh ITO as working electrode. I-t curve of the solution of complex **1** using a fresh ITO as working electrode was shown for comparison.

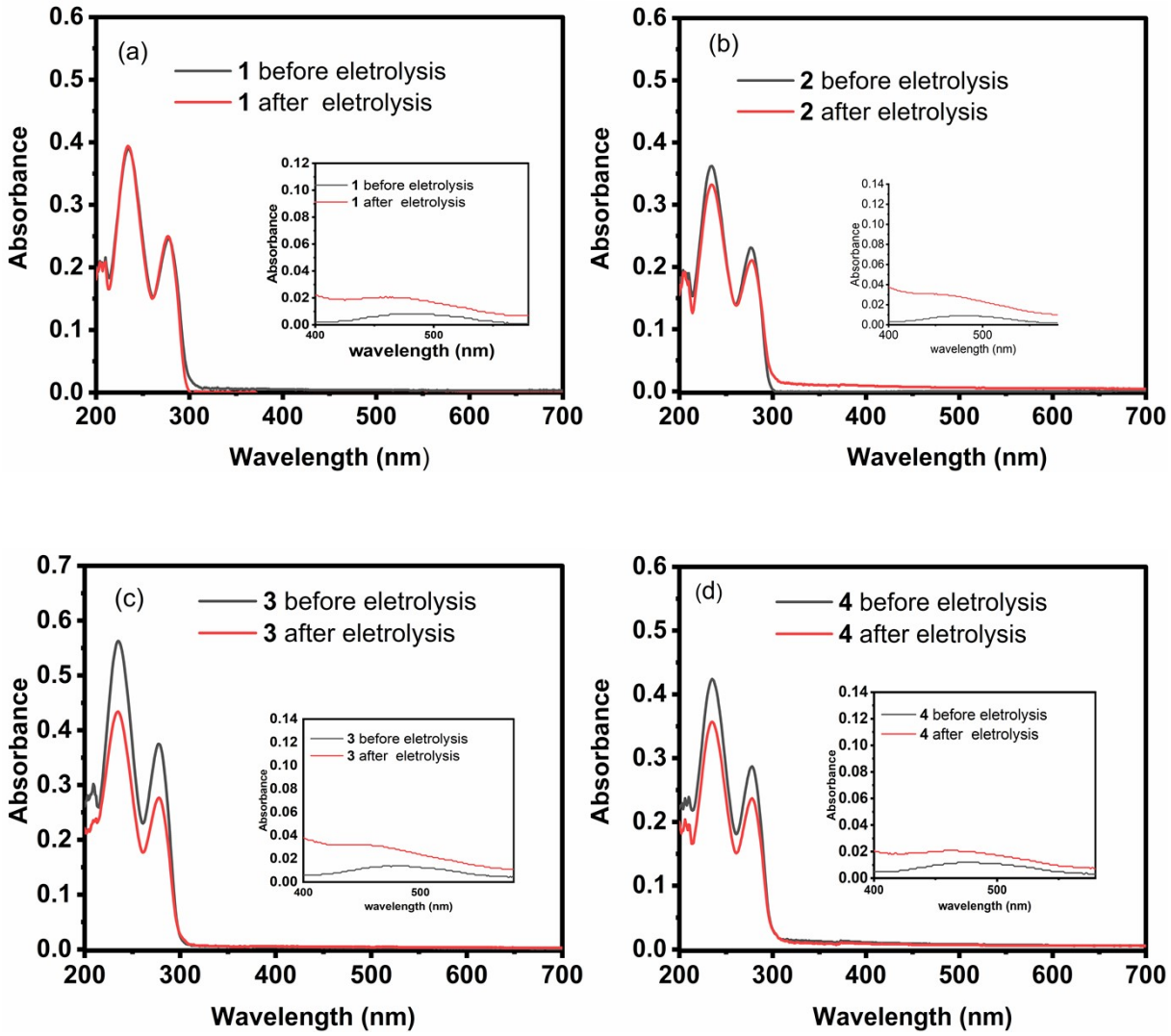


Fig. S12 UV-vis spectra of (a) **1**, (b) **2**, (c) **3** and (d) **4** in pH 7.0 0.1 M NaOAc-HOAc solution before (black line) and after (red line) CPE at 1.40 V. Concentration of sample: 1.0 mM.

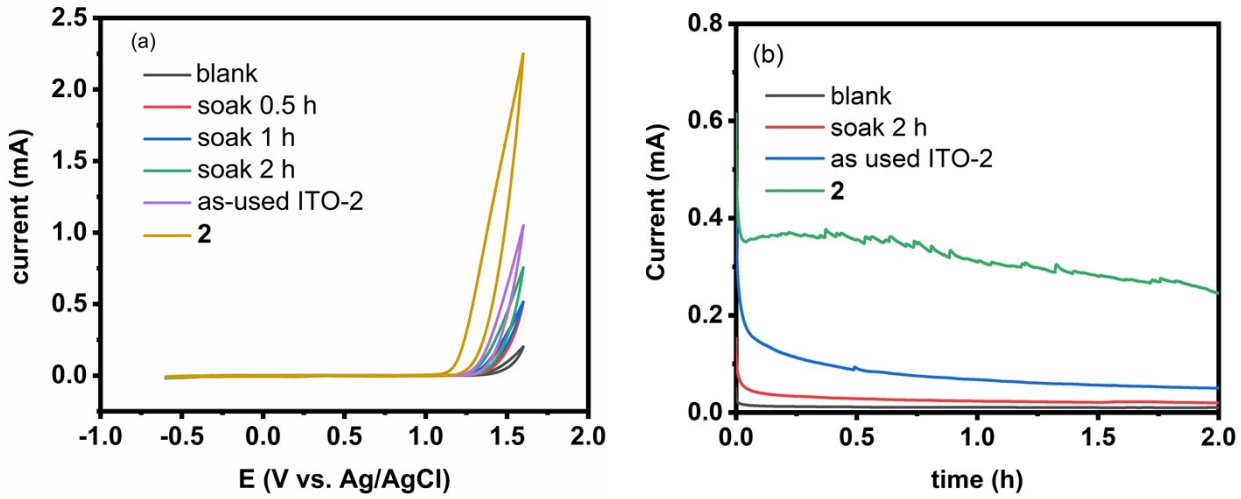


Fig. S13 (a) CVs in pH 7 0.1 M NaOAc-HOAc blank solution using ITO electrode soaked in the solution of **2** (0.4 mM) for different time as working electrodes, using the rinsed ITO electrode after the electrolysis of **2** at 1.40 V for 2 hours (as used ITO-2) as working electrode, using a fresh ITO as working electrode. CV of the solution of complex **2** using a fresh ITO as working electrode was shown for comparison. Scan rate: 100 mV $s^{-1}$. (b) I-t curves obtained from CPE at 1.40 V in the pH 7 0.1 M NaOAc-HOAc blank solution using ITO electrode soaked in the solution of **2** (0.4 mM) for 2 hours as working electrode, using the rinsed ITO electrode after the electrolysis of **2** at 1.40 V for 2 hours (as used ITO-2) as working electrode, using a fresh ITO as working electrode. I-t curve of the solution of complex **2** using a fresh ITO as working electrode was shown for comparison.

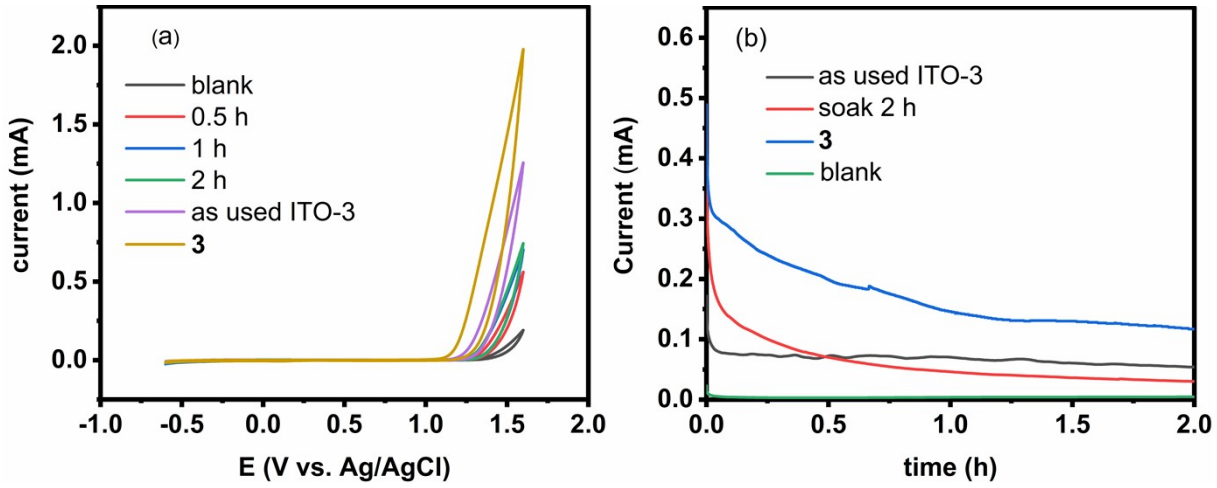


Fig. S14 (a) CVs in pH 7 0.1 M NaOAc-HOAc blank solution using ITO electrode soaked in the solution of **3** (0.4 mM) for different time as working electrodes, using the rinsed ITO electrode after the electrolysis of **3** at 1.40 V for 2 hours (as used ITO-3) as working electrode, using a fresh ITO as working electrode. CV of the solution of complex **3** using a fresh ITO as working electrode was shown for comparison. Scan rate: 100 mV $s^{-1}$. (b) I-t curves obtained from CPE at 1.4 V in the pH 7 0.1 M NaOAc-HOAc blank solution using ITO electrode soaked in the solution of **3** (0.4 mM) for 2 hours as working electrode, using the rinsed ITO electrode after the electrolysis of **3** at 1.40 V for 2 hours (as used ITO-3) as working electrode, using a fresh ITO as working electrode. I-t curve of the solution of complex **3** using a fresh ITO as working electrode was shown for comparison.

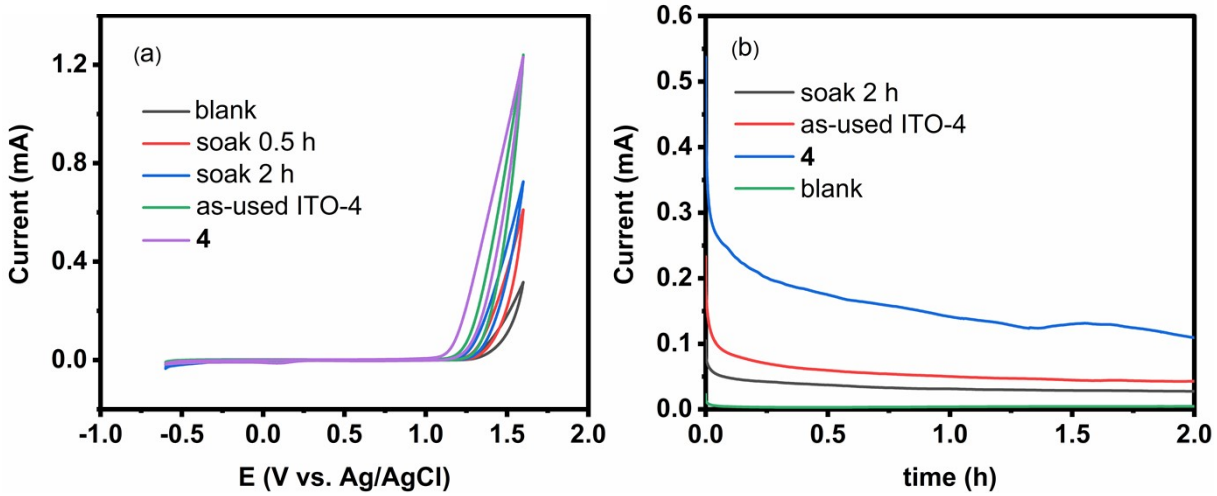


Fig. S15 (a) CVs in pH 7 0.1 M NaOAc-HOAc blank solution using ITO electrode soaked in the solution of **4** (0.4 mM) for different time as working electrodes, using the rinsed ITO electrode after the electrolysis of **4** at 1.40 V for 2 hours (as used ITO-4) as working electrode, using a fresh ITO as working electrode. CV of the solution of complex **4** using a fresh ITO as working electrode was shown for comparison. Scan rate: 100 mV $s^{-1}$. (b) I-t curves obtained from CPE at 1.4 V in the pH 7 0.1 M NaOAc-HOAc blank solution using ITO electrode soaked in the solution of **4** (0.4 mM) for 2 hours as working electrode, using the rinsed ITO electrode after the electrolysis of **4** at 1.40 V for 2 hours (as used ITO-4) as working electrode, using a fresh ITO as working electrode. I-t curve of the solution of complex **4** using a fresh ITO as working electrode was shown for comparison.

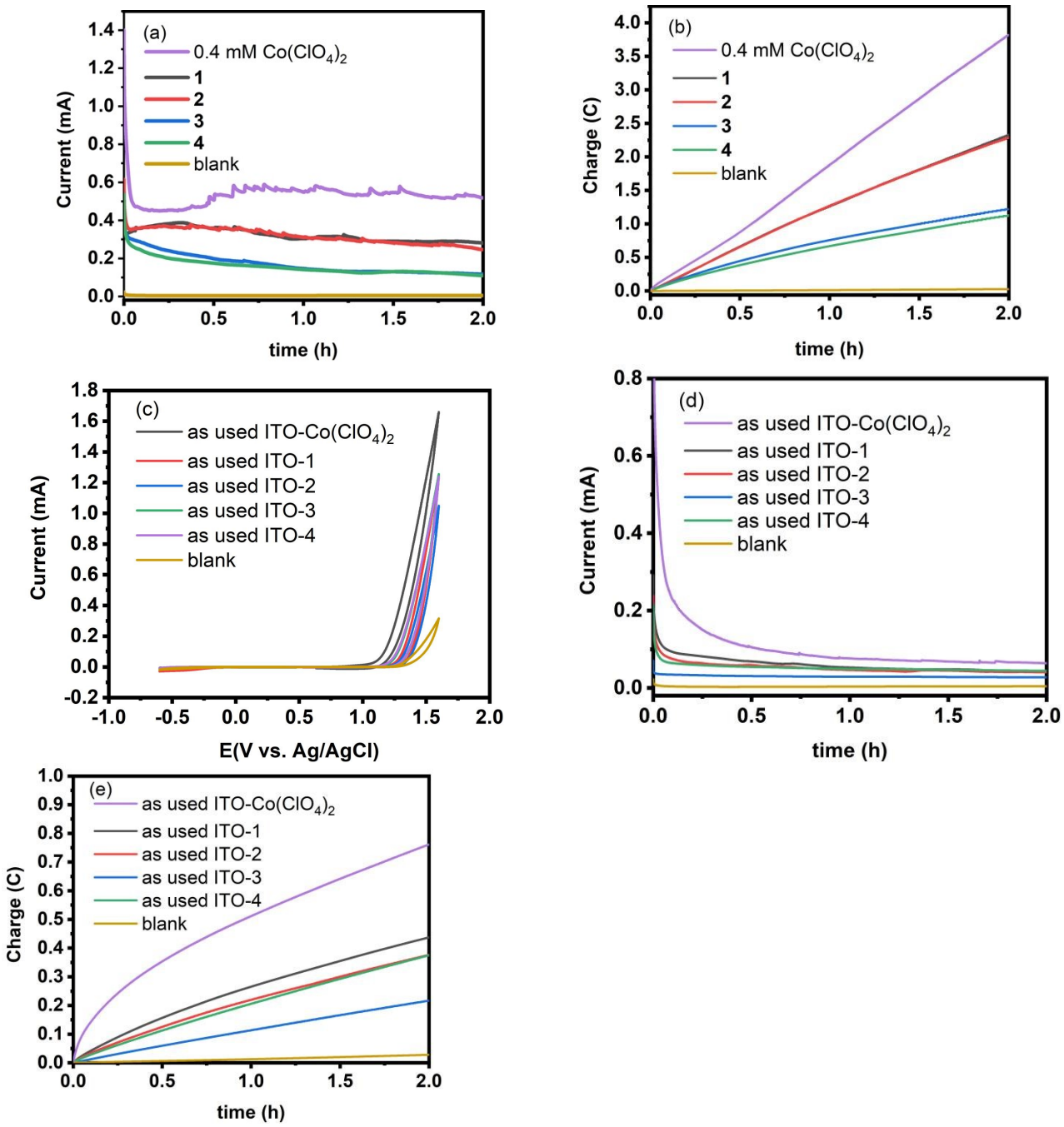


Fig. S16 (a) I–t curves and (b) charge buildup during CPE in pH 7.0 0.1 M NaOAc–HOAc solutions of complexes **1**-**4** and $Co(ClO_4)_2$ using ITO as working electrode at 1.40 V. Sample concentration: 0.4 mM. (c) CVs in pH 7.0 0.1 M NaOAc-HOAc blank solution using the rinsed ITO electrodes after the electrolysis of complexes **1**-**4** and $Co(ClO_4)_2$ at 1.40 V for 2 hours as working electrodes, using a fresh ITO as working electrode. Scan rate: 100 $mV.s^{-1}$. (d) I-t curves and (e) charge buildup obtained from CPE at 1.40 V in pH 7.0 0.1 M NaOAc-HOAc blank solution using the rinsed ITO electrodes after the electrolysis of complexes **1**-**4** and $Co(ClO_4)_2$ at 1.40 V for 2 hours as working electrodes, using a fresh ITO as working electrode.

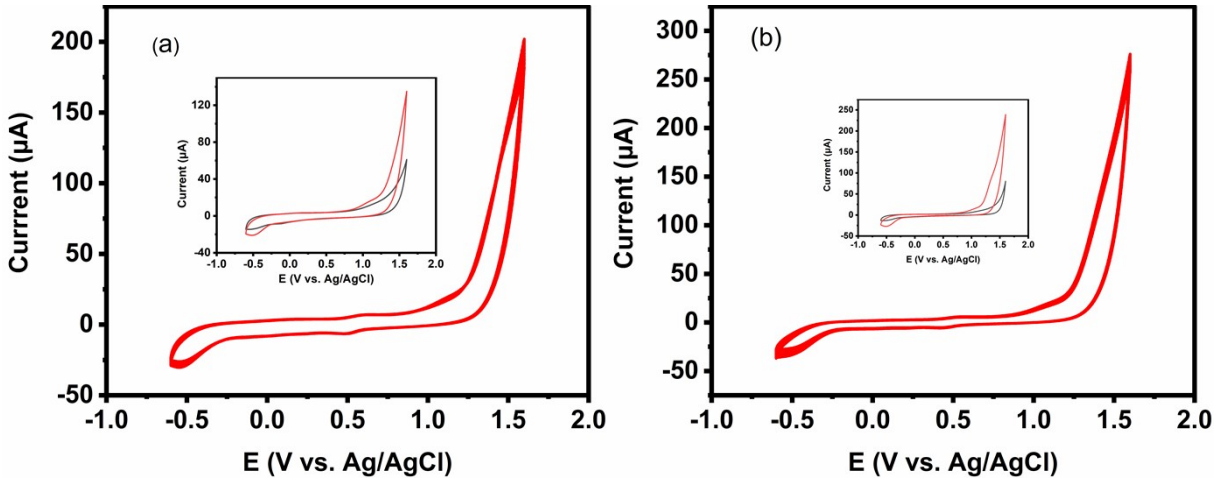


Fig. S17 Consecutive CVs (20 cycles) of (a) **1** and (b) **3** in pH 7.0 0.1 M NaOAc-HOAc solution. Concentration of sample: 0.4 mM. Inset: CVs in the blank pH 7.0 0.1 M NaOAc-HOAc solution using a fresh glassy carbon electrode as working electrode (black line) and using the electrode after 20 cycles which was rinsed but not polished as working electrode (red line). Scan rate: 100 mV $s^{-1}$.

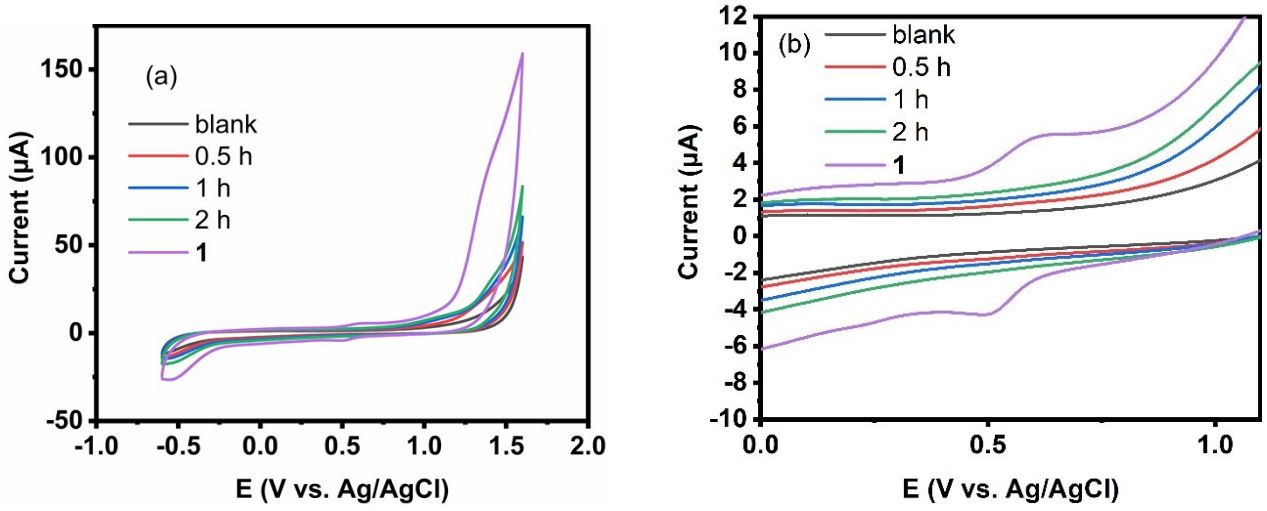


Fig. S18 (a) CVs in blank pH 7.0 0.1 M NaOAc-HOAc solution using glassy carbon electrode soaked in the solution of **1** (0.4 mM) for different time as working electrodes, using a fresh glassy carbon as working electrode (blank). CV of the solution of complex **1** was shown for comparison. Scan rate: 100 mV $s^{-1}$. (b) Magnified views of CVs in (a) in the potential range 0~1.10 V.

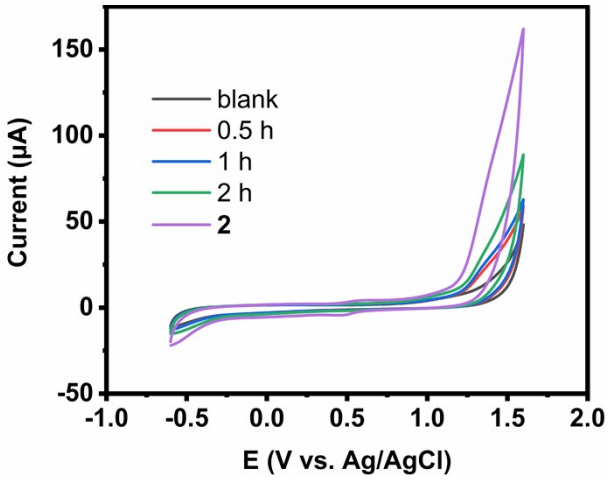


Fig. S19 (a) CVs in bank pH 7 0.1 M NaOAc-HOAc solution using glassy carbon electrode soaked in the solution of **2** (0.4 mM) for different time as working electrodes, using a fresh glassy carbon as working electrode (blank). CV of the solution of complex **2** was shown for comparison. Scan rate: 100 $mVs^{-1}$.

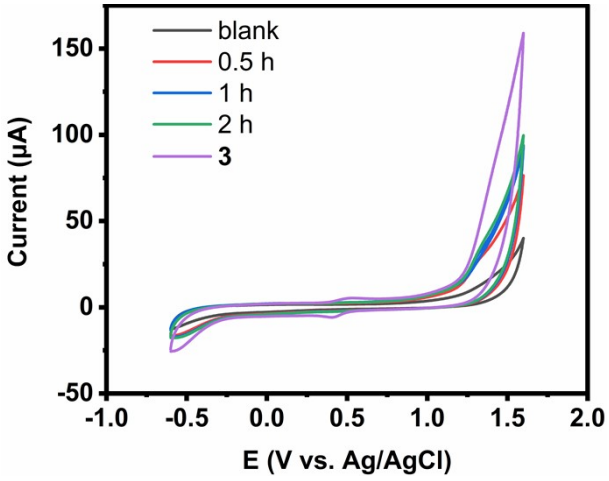


Fig. S20 CVs in blank pH 7 0.1 M NaOAc-HOAc solution using glassy carbon electrode soaked in the solution of **3** (0.4 mM) for different time as working electrodes, using a fresh glassy carbon as working electrode (blank). CV of the solution of complex **3** was shown for comparison. Scan rate: 100 $mVs^{-1}$.

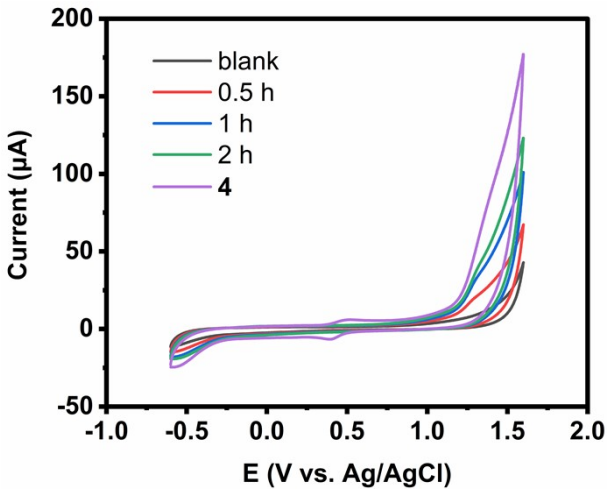


Fig. S21 CVs in blank pH 7.0 0.1 M NaOAc-HOAc solution using glassy carbon electrode soaked in the solution of **4** (0.4 mM) for different time as working electrodes, using a fresh glassy carbon as working electrode (blank). CV of the solution of complex **4** was shown for comparison. Scan rate: 100 mV $s^{-1}$.

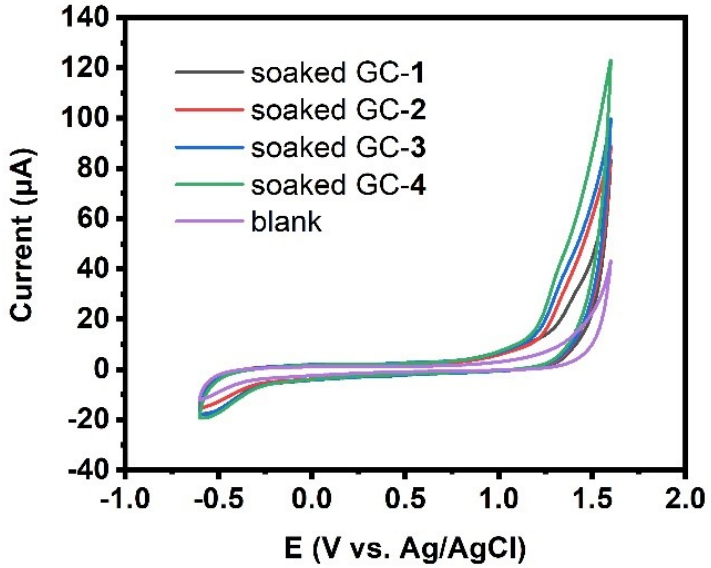


Fig. S22 CVs in blank pH 7.0 0.1 M NaOAc-HOAc solution using glassy carbon electrode soaked in the solutions of **1**-**4** (0.4 mM) for 2 hours as working electrodes (socked GC-1 for complex **1**, socked GC-2 for complex **2**, socked GC-3 for complex **3**, socked GC-4 for complex **4**). The CV using a fresh glassy carbon as working electrode (blank) was given for comparison.

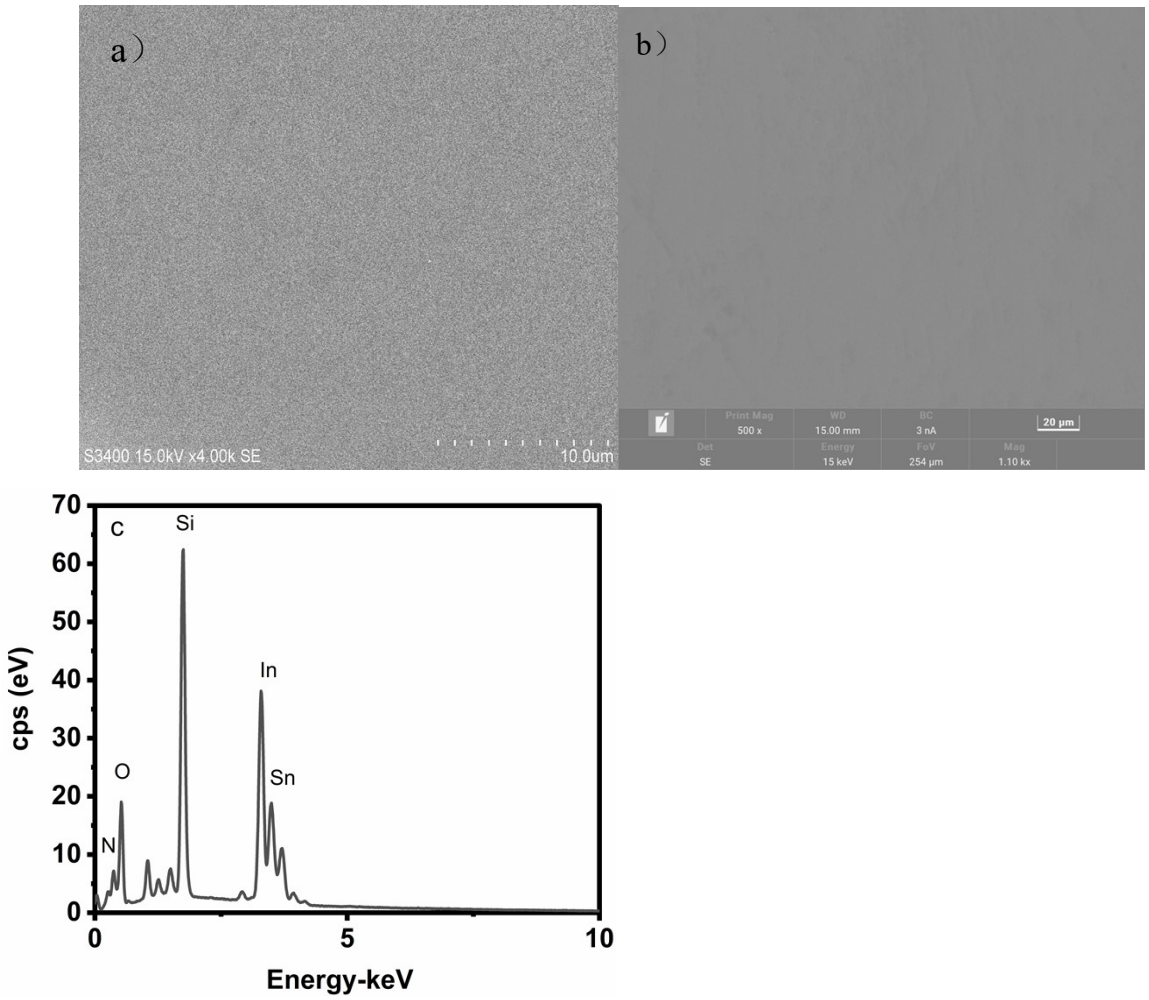


Fig. S23 a) SEM image of a fresh ITO electrode. b) SEM image and c) EDX spectrum of the ITO electrode obtained from the electrolysis of **1** (0.4 mM) in pH 7.0 0.1 M NaOAc-HOAc solution at 1.40 V for 2 hrs (as-used ITO-1).

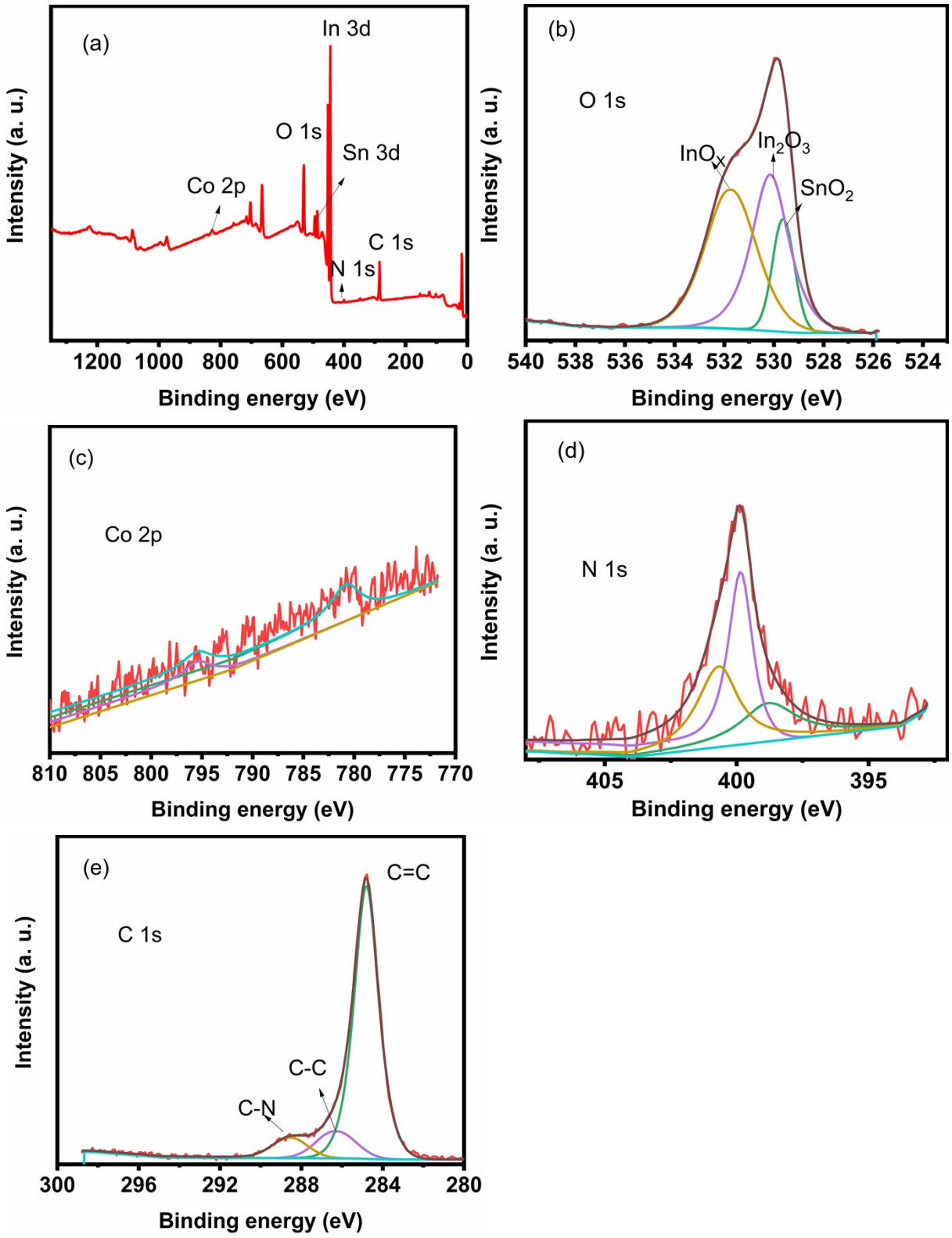


Fig. S24 XPS of the ITO electrode obtained from the electrolysis of **1** (0.4 mM) in pH 7.0 0.1 M NaOAc-HOAc solution at 1.40 V for 2 hrs (as-used ITO-1). a) the survey spectrum, b) high-resolution XPS of O 1s region, c) high-resolution XPS of Co 2p region, d) XPS of N 1s region, e) high-resolution XPS of C 1s region.

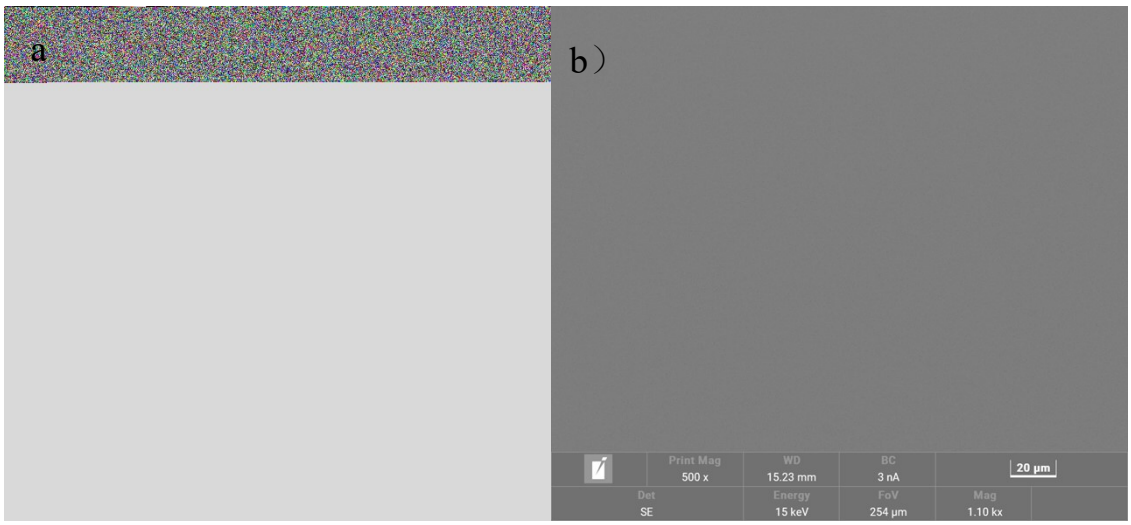


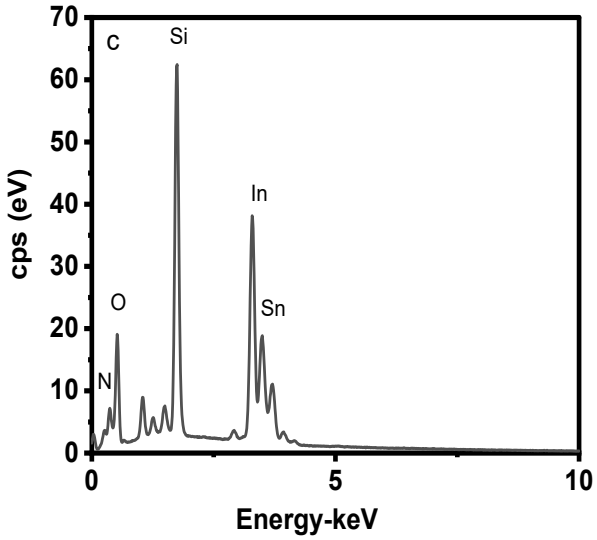


Fig. S25 a) SEM image of a fresh ITO electrode. b) SEM image and c) EDX spectrum of the ITO electrode obtained from soaking in pH 7.0 0.1 M NaOAc- HOAc solution of **1** for 2 hrs

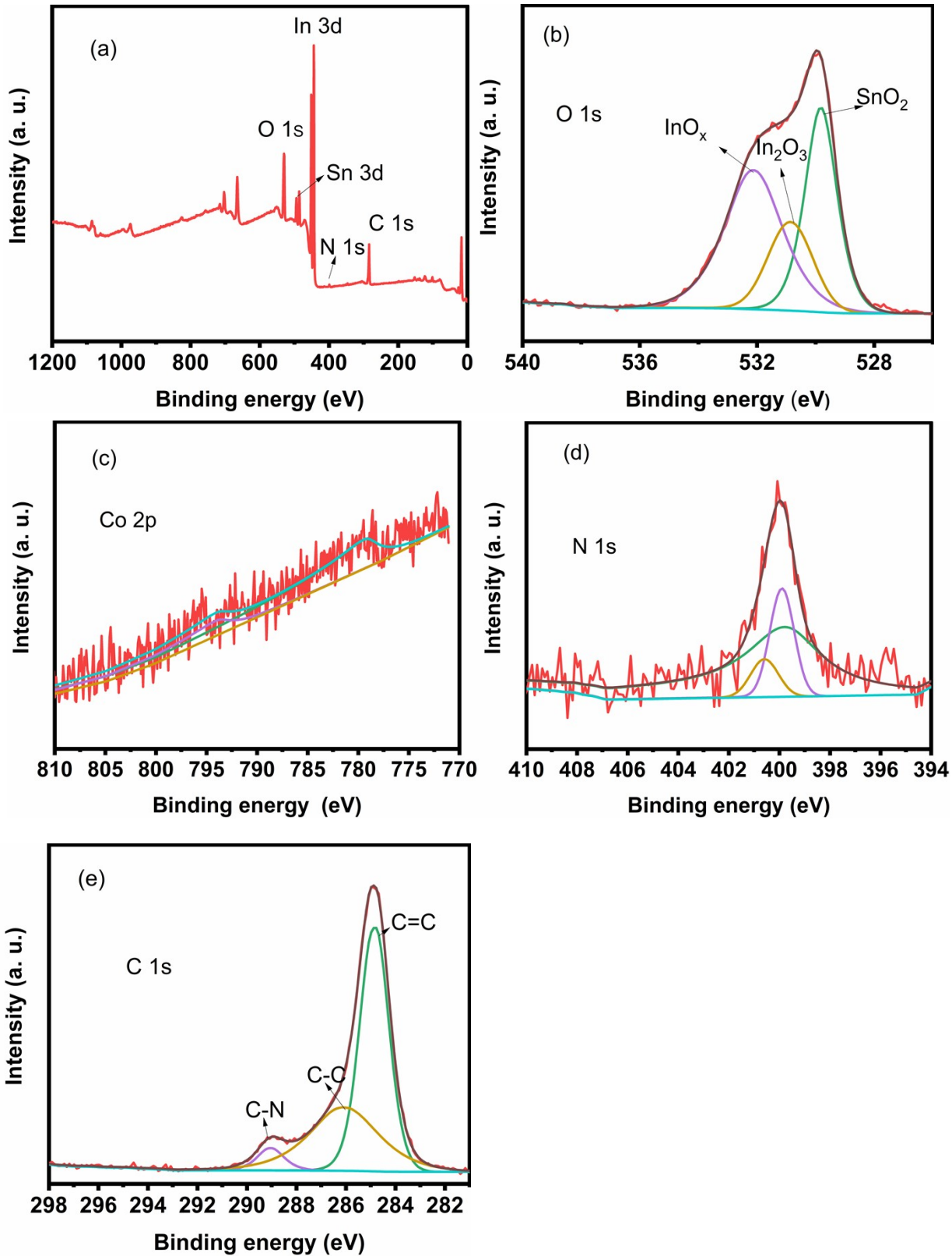


Fig. S26 XPS of the ITO electrode after soaking in pH 7.0 0.1 M NaOAc-HOAc solution of **1** (0.4 mM) for 2 hrs: a) The survey data, b) high-resolution XPS of O 1s region, c) high-resolution XPS of Co 2p region, d) high-resolution XPS of N 1s region, e) high-resolution XPS of C 1s region.

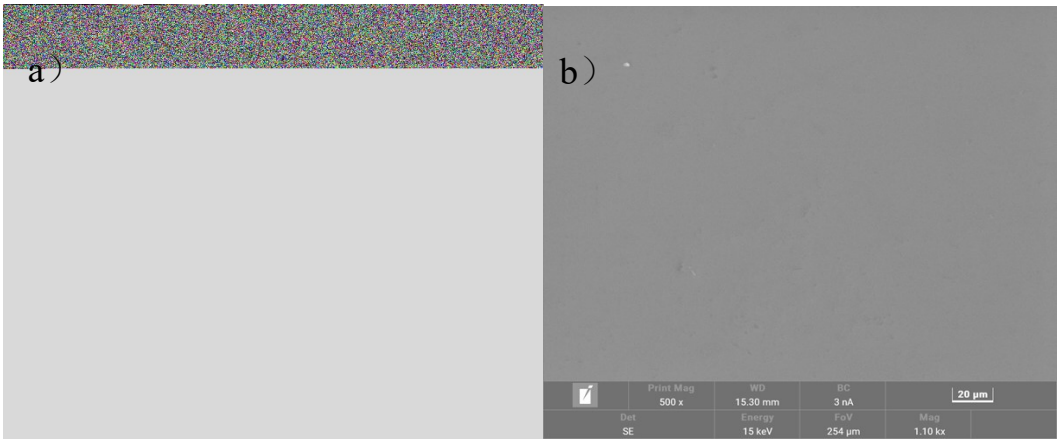


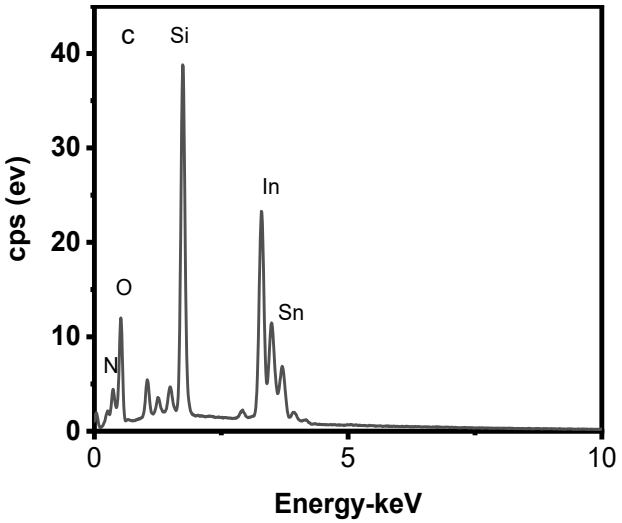


Fig. S27 a) SEM image of a fresh ITO electrode. b) SEM image and c) EDX spectrum of the ITO electrode obtained from the electrolysis of **3** (0.4 mM) in pH 7.0 0.1 M NaOAc-HOAc solution at 1.40 V for 2 hrs (as-used ITO-3).

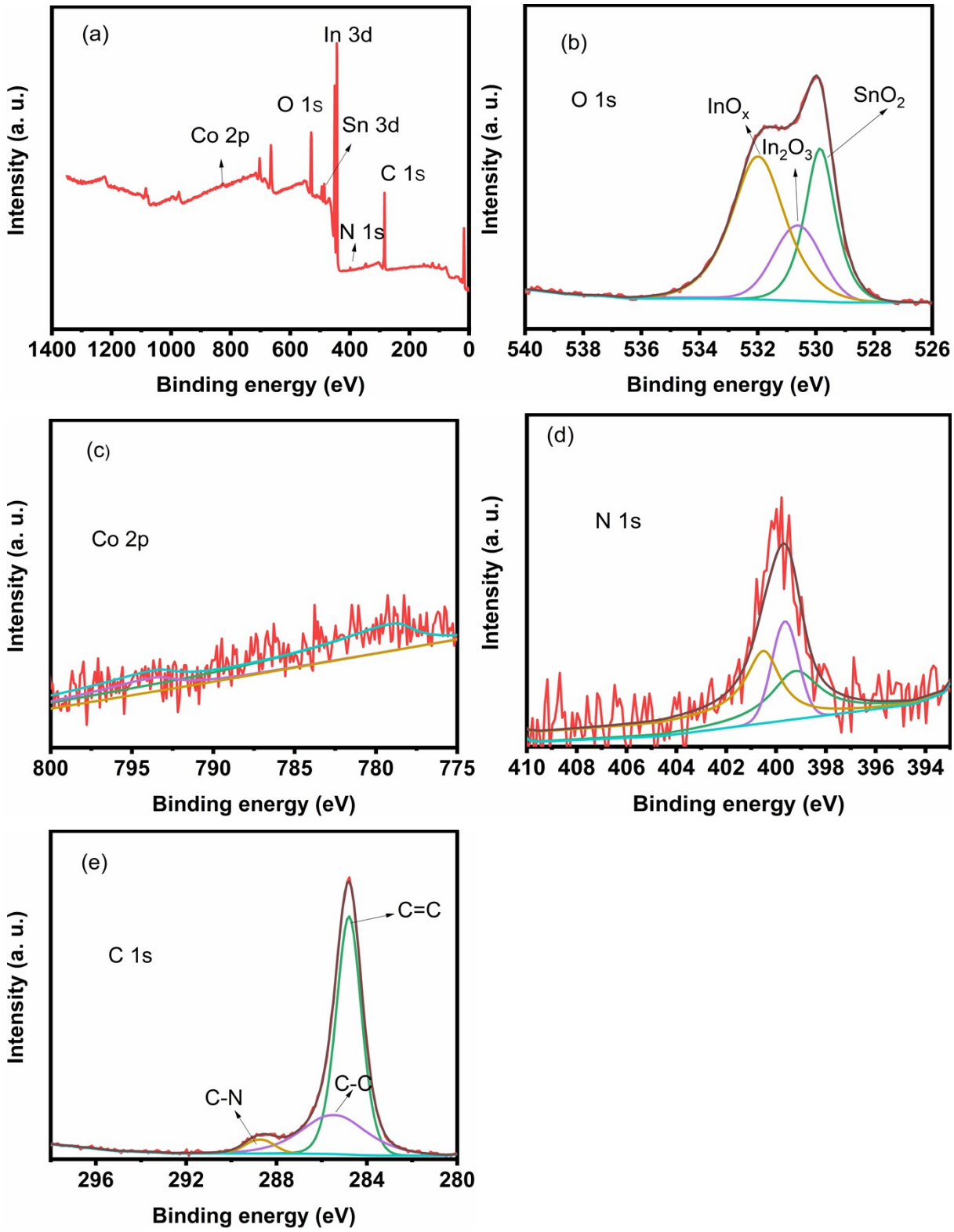


Fig. S28 XPS of the ITO electrode obtained from the electrolysis of **3** (0.4 mM) in pH 7.0 0.1 M NaOAc-HOAc solution at 1.40 V for 2 hrs (as-used ITO-3). a) the survey spectrum, b) high-resolution XPS of O 1s region, c) high-resolution XPS of Co 2p region, d) XPS of N 1s region, e) high-resolution XPS of C 1s region.

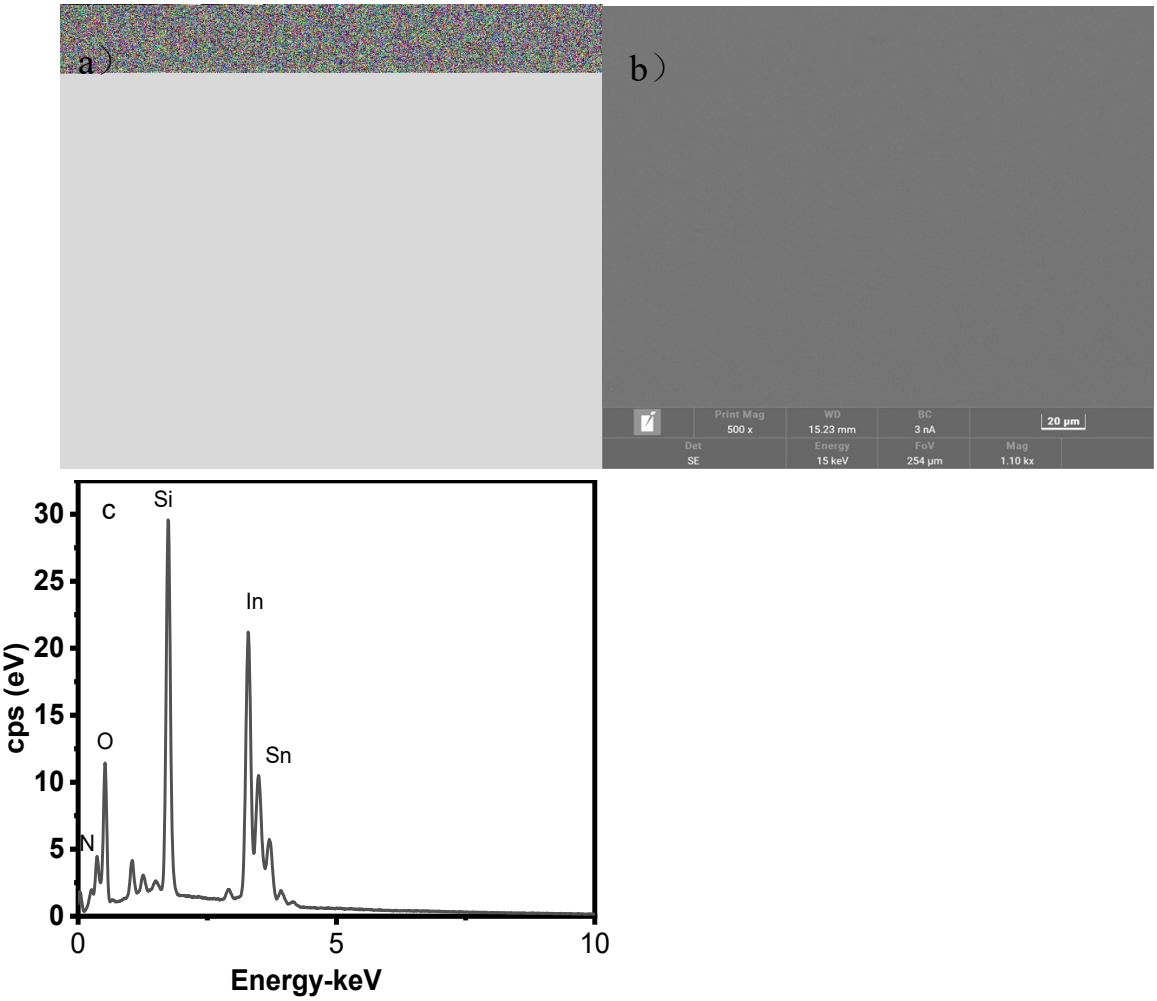


Fig. S29 a) SEM image of a fresh ITO electrode. b) SEM image and c) EDX spectrum of the ITO electrode obtained from soaking in pH 7.0 0.1 M NaOAc-HOAc solution of **3** for 2 hrs.

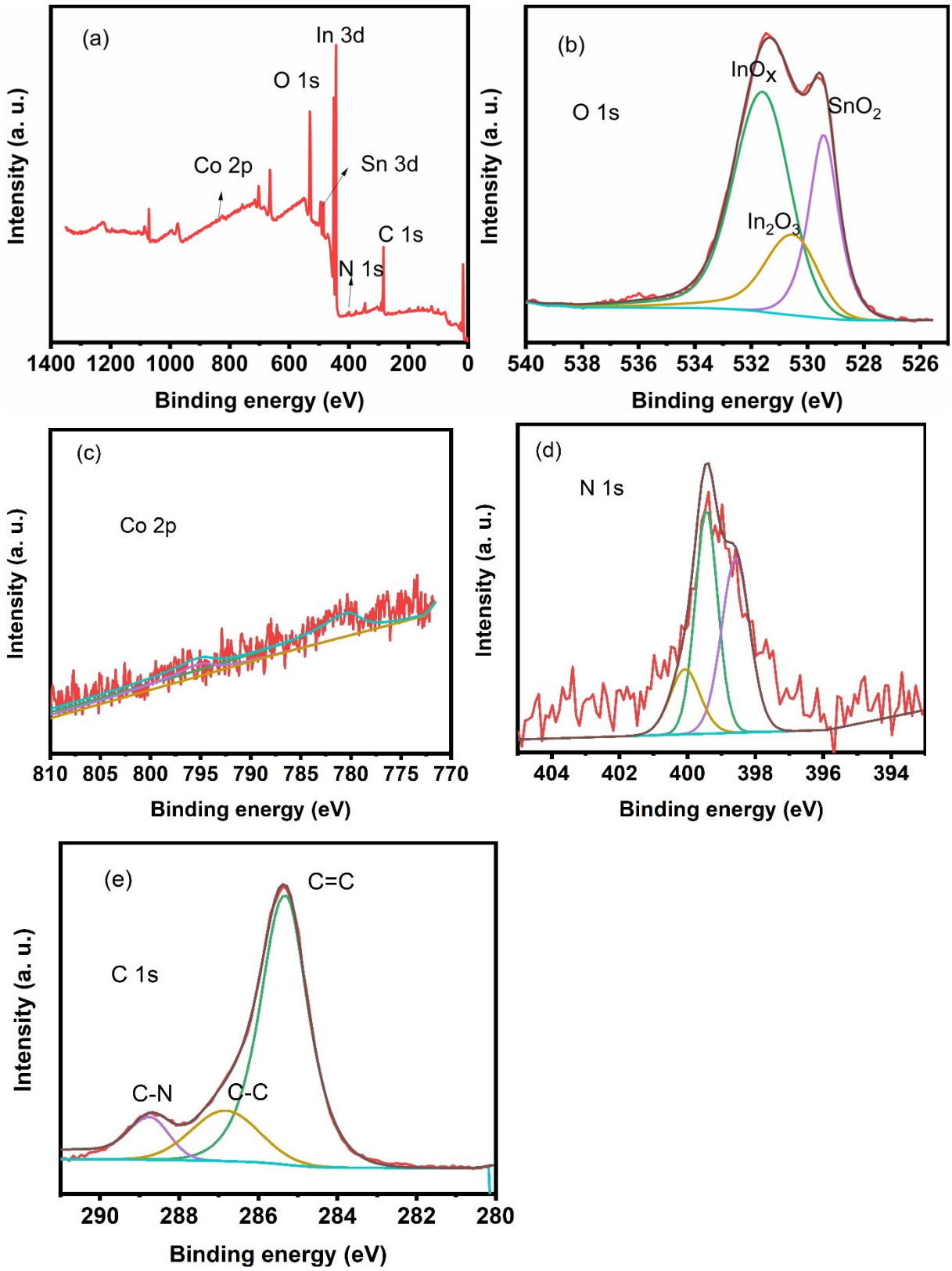


Fig. S30 XPS of the ITO electrode after soaking in pH 7.0 0.1 M NaOAc-HOAc solution of **3** (0.4 mM) for 2 hrs: a) The survey data, b) high-resolution XPS of O 1s region, c) high-resolution XPS of Co 2p region, d) high-resolution XPS of N 1s region, e) high-resolution XPS of C 1s region.

**References**


[S1] Y. F. Su, W. Z. Luo, W. Q. Lin, Y. B. Su, Z. J. Li, Y. J. Yuan, J. F. Li, G. H. Chen, Z. Li, Z. T. Yu, *Angew. Chem., Int. Ed.*, 2022, **61**, e202201430.

[S2] H. Sun, Y. Han, H. Lei, M. Chen, R. Cao, *Chem. Commun*., 2017, **53**, 6195.

[S3] D. Wang, J. T. Groves, *Proc. Natl. Acad. Sci. U.S. A*., 2013, **110**, 15579.

[S4] H. Zheng, H. Ye, T. Xu, K. Zheng, X. Xie, B. Zhu, X. Wang, J. Lin, Z. Ruan, *New. J. Chem*., 2022, **46**, 7522.

[S5] D. K. Dogutan, R. McGuire, D. G. *Nocera, J. Am. Chem. Soc*., 2011, **133**, 9178.

[S6] S. Biswas, S. Bose, J. Debgupta, P. Das, A. N. Biswas, *Dalton Trans.*, 2020, **49**, 7155.

[S7] H. A. Younus, N. Ahmad, A. H. Chughtai, M. Vandichel, M. Busch, K. Van Hecke, M. Yusubov, S. Song, F. Verpoort, *ChemSusChem*., 2017, **10**, 862.

[S8] D. J. Wasylenko, C. Ganesamoorthy, J. Borau-Garcia, C. P. Berlinguette, *Chem. Commun*., 2011, **47**, 4249.

[S9] Z. Q. Wang, L. Z. Tang, Y. X. Zhang, S. Z. Zhan, J. S. Ye, *J. Power Sources*, 2015, **287**, 50.

[S10] H. Y. Du, S. C. Chen, X. J. Su, L. Jiao, M. T. Zhang, *J. Am. Chem. Soc*., 2018, **140**, 1557.

[S11] H. Lei, A. Han, F. Li, M. Zhang, Y. Han, P. Du, W. Lai, R. Cao, *Phys. Chem. Chem. Phys.,* 2014, **16**, 1883.

[S12] D. Das, S. Pattanayak, K. K. Singh, B. Garai, S. S. Gupta, *Chem. Commun*., 2016, **52**, 11787.

[S13] N. D. McMillion, A. W. Wilson, M. K. Goetz, M. C. Chang, C. C. Lin, W. J. Feng, C. C. L. McCrory, J. S. Anderson, I*norg. Chem*., 2019, **58**, 1391.